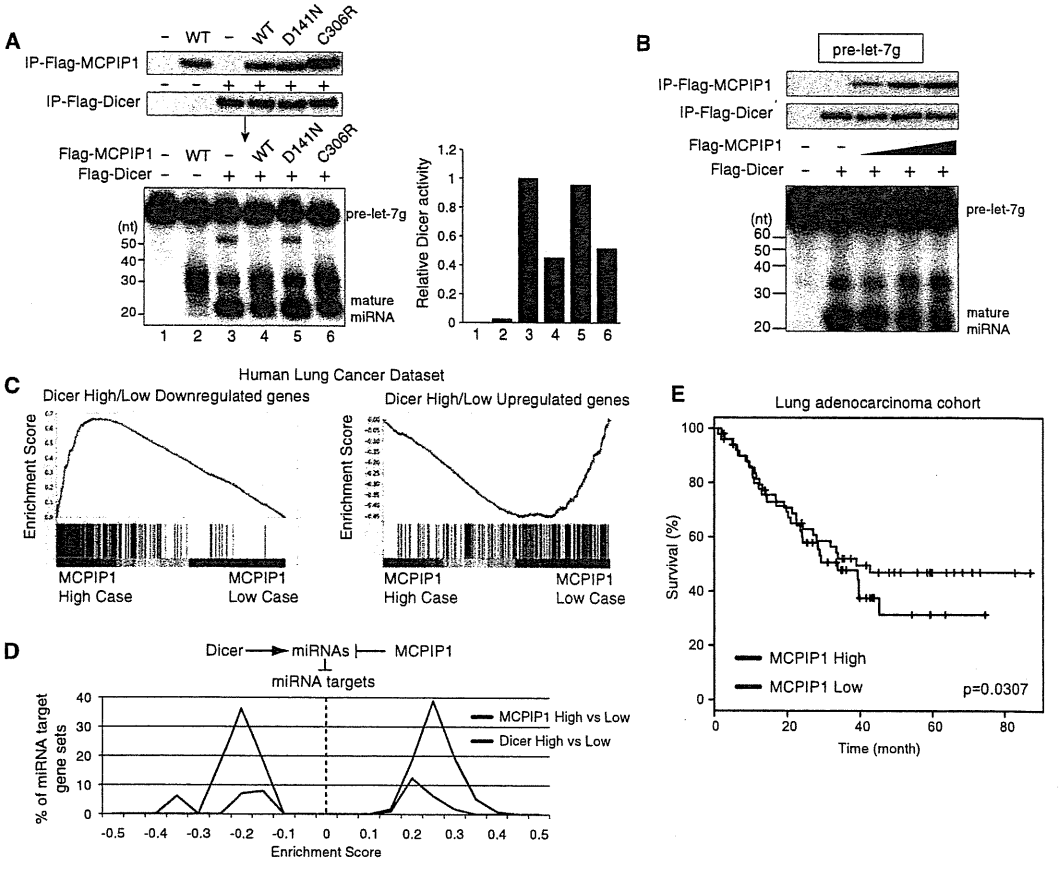

Figure 4. Antagonism between MCPIP1 Ribonuclease and Dicer and Its Implication in Human Cancer

(A and B) In vitro competition analysis using FLAG-Dicer, FLAG-MCPIP1 mutants (A), or increased amounts of FLAG-MCPIP1 (B) and radiolabeled pre-let-7g. Cleaved mature miRNAs are quantified as relative Dicer activity (A, right).

(C) Gene set enrichment analysis (GSEA) for genes negatively or positively associated with Dicer expression ("Dicer High/Low Downregulated or Upregulated genes"), along with the patients with high and low MCPIP1 expression ("MCPIP1 High Case" versus "MCPIP Low Case"), in the cohort of lung adenocarcinoma patients (Bild et al., 2006). Genes negatively or positively associated with Dicer expression were enriched in MCPIP1-High group and MCPIP1-Low group, respectively.

(D) Global histogram showing distribution of GSEA enrichment scores for the putative miRNA target gene sets in the lung adenocarcinoma cohort (Bild et al., 2006). In the comparison between Dicer-High and -Low groups, large proportion of miRNA target gene sets were underrepresented in Dicer-High group. In contrast, opposite asymmetrical distribution was observed in the comparison according to MCPIP1 expression, supporting the antagonism between Dicer and MCPIP1.

(E) Kaplan-Meier plots representing the survival probability in the same dataset, according to low or high MCPIP1 expression levels. The log-rank test p value reflects the significance of the association between high MCPIP1 expression and poor prognosis. See also Figure S4.

cleavage by MCPIP1 in vitro (Figure 6D), strengthening the importance of terminal loop as a target of MCPIP1.

While MCPIP1 has recently been shown to promote the mRNA decay of IL-6 (Matsushita et al., 2009), we noticed that the target element of IL-6 3′ UTR forms a stem-loop structure similar to pre-miRNAs (Matsushita et al., 2009; Paschoud et al., 2006) (Figure 6C, right). We similarly cloned the IL-6 3′ UTR fragments cleaved by MCPIP1 in vitro, and found that the ends of recovered 5′ and 3′ fragments were distributed in 5′- and 3′-franking regions of the hairpin structure, respectively (Figure S6D), supporting the idea that MCPIP1 preferentially targets the hairpin structure. We then investigated structural features of MCPIP1 target RNAs by generating a range of pre-miRNA mutants with various lengths of stem and terminal loop. As a result, deletion analysis showed that MCPIP1 could cleave pre-miRNA mutants with various stem lengths (Figures 6E and S6E), while deletion of the loop region affected MCPIP1 action in vitro, and MCPIP1 could not cleave pre-miRNA mutants without a loop region (Figures 6F and S6F, see d5–7 mutants). These findings thus suggest that MCPIP1 potentially controls the destinies of various hairpin RNAs. This notion parallels the finding that the Drosha-DGCR8 complex cleaves the hairpin structure in DGCR8 mRNA, as well as pri-miRNAs (Han et al., 2009). These observations imply the presence of dynamic crosstalk between the pathways for mRNA stability control and miRNA biogenesis.

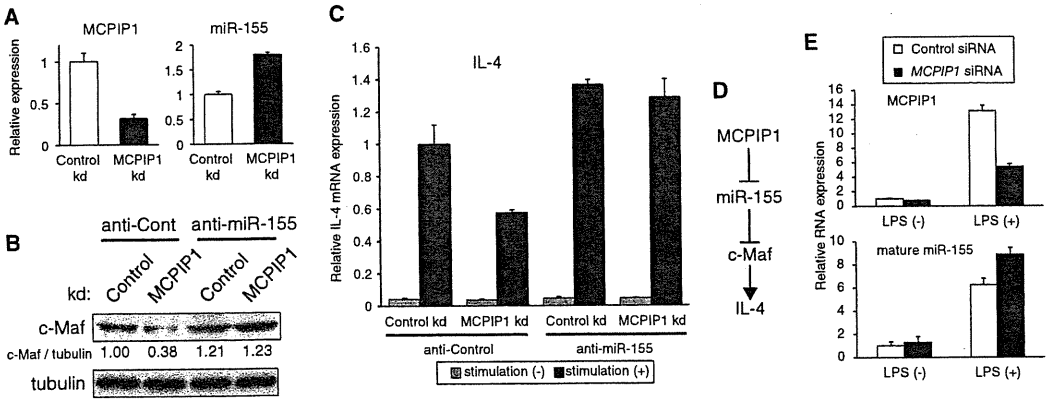

Figure 5. Modulation of miR-155/c-Maf Axis by MCPIP1

(A) miR-155 upregulation by MCPIP1 knockdown in Jurkat cells. Jurkat cells were transduced with MCPIP1 knockdown lentivirus vector (MCPIP1 kd) and analyzed by qRT-PCR analysis.

(B) miR-155-dependent c-Maf suppression by MCPIP1 depletion, as assessed by immunoblot analysis of c-Maf under a combination of MCPIP1 knockdown and transfection of anti-miR-155 inhibitor in Jurkat cells.

(C) Effects of MCPIP1 and miR-155 suppression on IL-4 induction by stimulation with PMA and ionomycin. Jurkat cells were prepared in the same combination as in (B) and analyzed by qRT-PCR analysis.

(D) Relationship of MCPIP1/miR-155/c-Maf/IL-4 axis.

(E) Involvement of MCPIP1 in LPS-mediated miR-155 upregulation in THP-1 macrophage cells, as assessed by qRT-PCR analysis after transfection with control siRNA or *MCPIP1* siRNA. See also Figure S5. Error bars represent SEM.

Oligomerization of MCPIP1 Ribonuclease via the Vertebrate-Specific C Terminus

In our study, other MCPIP family proteins (MCPIP2, MCPIP3, and MCPIP4) showed little effect on miRNA activity in spite of the presence of the conserved NYN domain and CCCH motif (Figures 1A, 7A, and S7A). Together with the differential effects of C306R mutation on in vitro and in vivo activities of MCPIP1 (Figures 3D–3G), these observations raised the possibility that other domain(s) including CCCH motif, besides the NYN domain, could be important for the in vivo function of MCPIP1. Besides the NYN domain, the CCCH zinc-finger domain and proline rich domain are placed at the central region and C-terminal region of MCPIP1, respectively (Figure 7A). In *C. elegans* and *Drosophila*, a similar protein with MCPIP1, C30F12.1 and CG10889, respectively, is observed (Figure 7A). These molecules lack a proline-rich domain found in MCPIP1 C terminus, and the C terminus of vertebrate MCPIP2/3/4 also shows little similarity with the MCPIP1 C terminus, suggesting that the C terminus of MCPIP1 has emerged as a certain functional domain in the vertebrate MCPIP gene family (Figure 7A).

Previous studies have demonstrated that some RNases and RNase domains, including RNase A and RNase L, function in the oligomerized state (Bergdoll et al., 1997; Salehzada et al., 1993). RNase A has been shown to oligomerize via a proline-dependent arm exchange mechanism (Bergdoll et al., 1997). Dicer has also been shown to function through intramolecular dimerization of its two RNase III domains (Zhang et al., 2004).

On the basis of these findings, we examined the possibility of MCPIP1 oligomerization via the unconserved C-terminal region including the proline-rich domain. While human MCPIP1 was usually observed as a 66 kDa monomer, the protein was detected as a high molecular weight complex of about 200 kDa under chemical crosslinking by disuccinimidyl suberate (DSS) (Figure 7B). Blue native PAGE analysis revealed that overexpressed and endogenous MCPIP1 proteins mainly exist as complexes of about 200 kDa, and of about 220 kDa and 600–700 kDa, respectively (Figure 7C). Immunoprecipitation analysis also detected an additional band of FLAG-tagged MCPIP1 with about 400 kDa in blue native PAGE (Figure 7D). Since these FLAG-MCPIP1 complexes were coimmunoprecipitated with cointroduced HA-tagged MCPIP1 (Figures 7B and 7D), these complexes may represent oligomeric forms of MCPIP1. In addition, endogenous MCPIP1 complexes of about 220 kDa and 600–700 kDa showed higher molecular weights than two FLAG-tagged MCPIP1 complexes of 200 kDa and 400 kDa, suggesting the presence of additional partner protein(s) interacting with endogenous MCPIP1. The conventional immunoprecipitation experiments confirmed the association between FLAG-tagged and HA-tagged MCPIP1 molecules (Figure S7B) and revealed that this oligomerization required the C-terminal region (Figures S7C and S7E). In accordance with the results, these C-terminal deletion mutants also showed reduced miRNA suppressor activities (Figures 7F, 7G, S7D, and S7E). Furthermore, RNA immunoprecipitation analysis clarified that both the CCCH motif and vertebrate-specific C terminus are important for efficient interaction between MCPIP1 and pre-miRNA in vivo, although the NYN domain has a minor role in this aspect (Figure 7H). We further observed that D141N and C306R mutants showed little dominant-negative effects on the function of wild-type MCPIP1 both in vivo and in vitro (Figure S7F). Collectively, MCPIP1 harbors several functional domains to inhibit miRNA maturation efficiently (Figure 7I). The presence of the vertebrate-specific MCPIP1 C terminus suggests that the

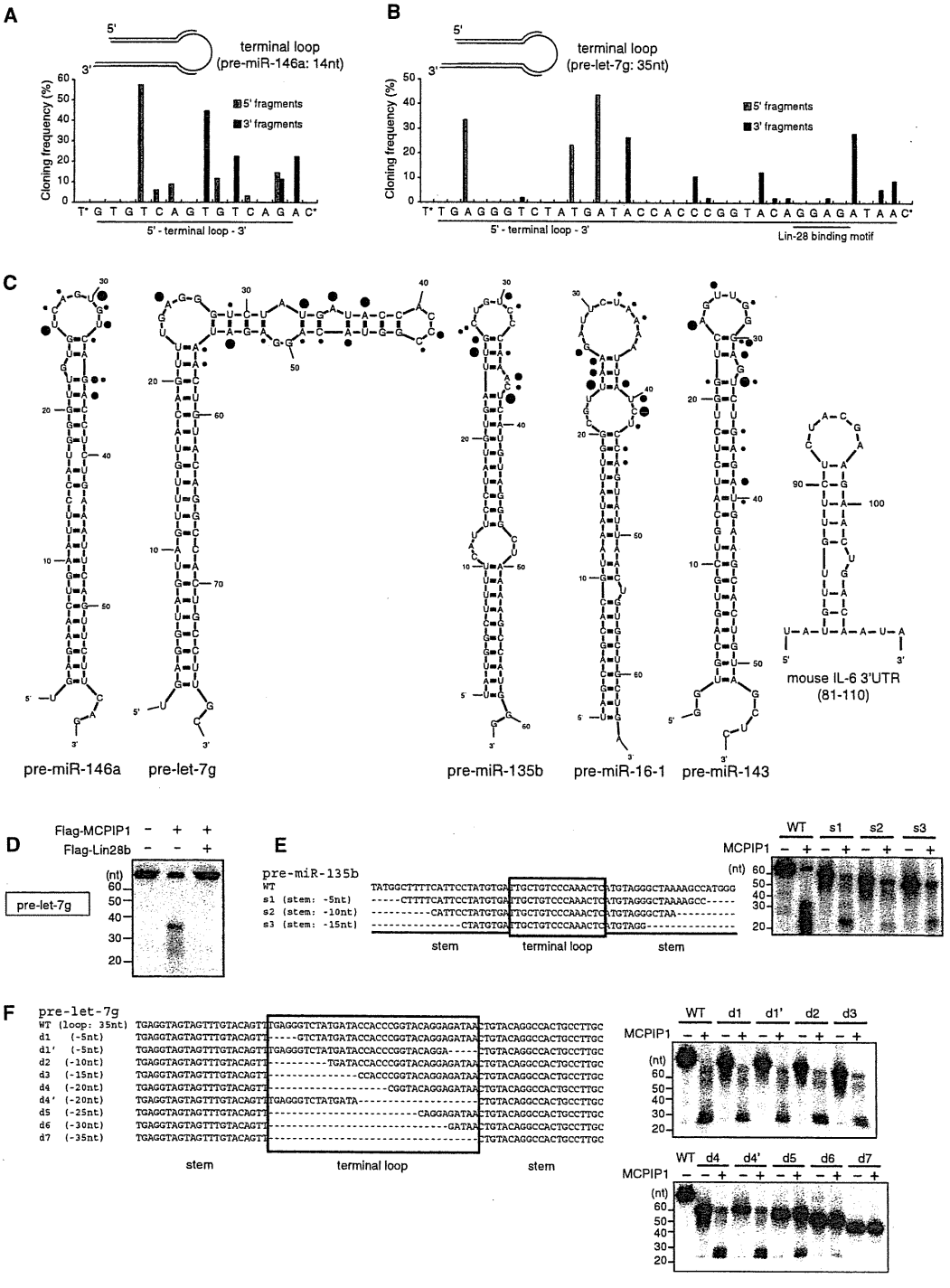

Figure 6. Targeting of the Terminal Loops of Pre-miRNAs by MCPIP1 Ribonuclease

(A and B) Cloning analysis of MCPIP1-cleaved pre-miRNA fragments. After in vitro cleavage reaction (90 min), the cleaved fragments of pre-miR-146a (A) and pre-let-7g (B) were cloned and sequenced. 5′ and 3′ fragments indicate the fragments composed of 5′ and 3′ mature miRNA strand and additional bases within the terminal loop, respectively. The data about pre-miR-135b, pre-miR-143, and pre-miR-16-1 are shown in Figures S6A–S6C.

(C) Comparison of the sequence analyses of MCPIP1-cleaved fragments (A and B and Figures S6A–S6C) and secondary structure prediction (Zuker, 2003). The ends of 5′ and 3′ fragments are indicated by blue and red circles, respectively. The structure of MCPIP1 target sequence of mouse *Il6* 3′ UTR (80–110) is also shown.

MCPIP family has evolved an anti-miRNA function of MCPIP1 in vertebrates.

DISCUSSION

Here we identified the CCCH zinc-finger ribonuclease MCPIP1 as an important RNase, which counteracts the productive miRNA biogenesis directed by two RNases, Drosha and Dicer (Figure 7J). It is poorly understood how the half-lives and absolute levels of mature miRNAs are determined, in comparison with advances concerning the mechanisms of miRNA production. Recent reports revealed that several nucleases, such as SDN in *Arabidopsis* and XRN-2 in *C. elegans*, degrade mature miRNAs (Chatterjee and Grosshans, 2009; Ramachandran and Chen, 2008). The present study first demonstrated that not only mature miRNAs but also pre-miRNAs are targets of active degradation to reduce miRNA activities. Considering that MCPIP1 expression dynamically changes during the inflammatory response (Liang et al., 2008a; Liang et al., 2008b), the rate of de novo miRNA synthesis might be actively regulated through the pre-miRNA decay by MCPIP1. Accordingly, global downregulation of miRNAs including miR-16 (as also demonstrated in Figure S5C) and overall shortening of mRNA 3′ UTRs have been observed along T cell activation (Sandberg et al., 2008; Wu et al., 2007).

Open questions remain regarding how MCPIP1 recognizes pre-miRNAs and preferentially inhibits the miRNA pathway and whether MCPIP1 uniformly acts on individual miRNAs. While further investigation is important, our trial analysis of RNA-IP/sequencing experiments suggested that the MCPIP1 D141N mutant interacts with a range of miRNA precursors and transcripts including IL6 (Figures S7G and S7H). On the other hand, the expression levels of externally expressed DGCR8 mRNA and IL-6 3′ UTR RNA both containing a hairpin structure decreased to about 50% by MCPIP1 overexpression (Figure S7I, left), as well as pre-miRNAs, but MCPIP1 knockdown only slightly upregulated the endogenous DGCR8 and IL-6 mRNA levels and also failed to show significant or consistent effects on other RNA species such as Alu and tRNAs (Figure S7I, right), in contrast to the effects on endogenous mature miRNAs. Considering that MCPIP1 decreased overexpressed pre-miRNAs by about half and their mature forms by about one-tenth (Figure 1), these results suggest that the miRNA biogenesis pathway is more susceptible to MCPIP1 regulation than other RNA species, maybe because of the requirement for stepwise collaboration of multiple maturation processes. Differential localization of MCPIP1 and various RNA species may also contribute to the strong inhibitory impact of MCPIP1 on the miRNA pathway. In addition, heterogenous effects of MCPIP1 knockdown on individual mature miRNAs (Figures 2G and 2H) might be attributable to intrinsic properties of MCPIP1, as influenced by preferential target structures/sequences and additional partner protein(s), or complexity of regulation of each miRNA modified by various factors, including pri-miRNA transcription, Drosha processing, cytoplasmic export, Dicer processing, existence of specific RNA-binding proteins, and miRNA stability regulation.

Lin-28 interacts with the terminal loop of let-7 precursor and specifically hinders let-7 maturation. In addition, several other RNA-binding proteins such as hnRNP A1 and KSRP also interact with the terminal loops of miRNA precursors and rather facilitate the processing of pri-miRNAs and/or pre-miRNAs. Considering that MCPIP1 targets the terminal loop of pre-miRNAs, these RNA-binding proteins might protect miRNA precursors from the degradation in addition to their intrinsic function in miRNA biosynthesis. Since the loop region is largely considered dispensable for the basic action of Drosha and Dicer, the evolutionarily conserved loops of many miRNA precursors might contain regulatory information for active degradation to differentially generate distinct miRNA species.

Our results demonstrated the importance of the C terminus for MCPIP1 function and its poor conservation between invertebrates and vertebrates (Figure 7). These findings suggest that the vertebrate MCPIP family has diversified and evolved an anti-miRNA function of MCPIP1. Although miRNA and RNAi pathways and their components are well conserved across a wide range of species, previous studies suggested certain evolutional differences, in particular from immunological aspects, as represented by different major antiviral mechanisms between plants/invertebrates and mammals, i.e., respectively, RNAi response and interferon (IFN) response (Umbach and Cullen, 2009). In addition, miRNAs encoded in certain mammalian viruses perturb host gene regulatory networks and there exist several mechanisms represented by RNase L and ZAP to avoid the promiscuity by viral-derived RNA species in vertebrate cells (Sadler and Williams, 2008). The presence of MCPIP1-mediated abortive processing machinery and diversity of MCPIP1-related genes, taken together with these findings, may therefore imply dynamic evolutional transition of RNA silencing system.

In the present study, we have intriguingly found an inverse correlation between MCPIP1 and Dicer function in human lung cancer cohorts (Figures 4C–4E and S4). Importantly, we observed an association of high MCPIP1 expression with poor survival, suggesting the usefulness of MCPIP1 as a prognostic marker. MCPIP1 upregulation by several inflammatory stimuli, including MCP1, might be partly attributable to global miRNA downregulation in cancer, in addition to reduced expression of Dicer and/or Drosha and mutations in TRBP and XPO5. Future studies may provide useful information about involvement of MCPIP1 in miRNA dysregulation in human malignancies and important insights for the efficiency of RNA-based therapeutics. In conclusion, the present work provides a clue for the comprehensive understanding of miRNA dynamics during the

(D) Effect of Lin-28b addition on MCPIP1 activity targeting pre-let-7g.
(E) Effect of the stem length of pre-miRNA on MCPIP1 activity. (Left) The sequences of deletion mutants of pre-miR-135b with various lengths of stem region. (Right) In vitro cleavage assay by coincubation of radiolabeled pre-miR-135b mutants and FLAG-MCPIP1 for 90 min.
(F) Effect of the terminal-loop length of pre-miRNA on MCPIP1 activity. (Left) The sequences of deletion mutants of pre-let-7g carrying a long terminal loop (35 nt). (Right) In vitro cleavage assay by coincubation of radiolabeled pre-let-7g mutants and FLAG-MCPIP1 for 120 min. See also Figure S6.

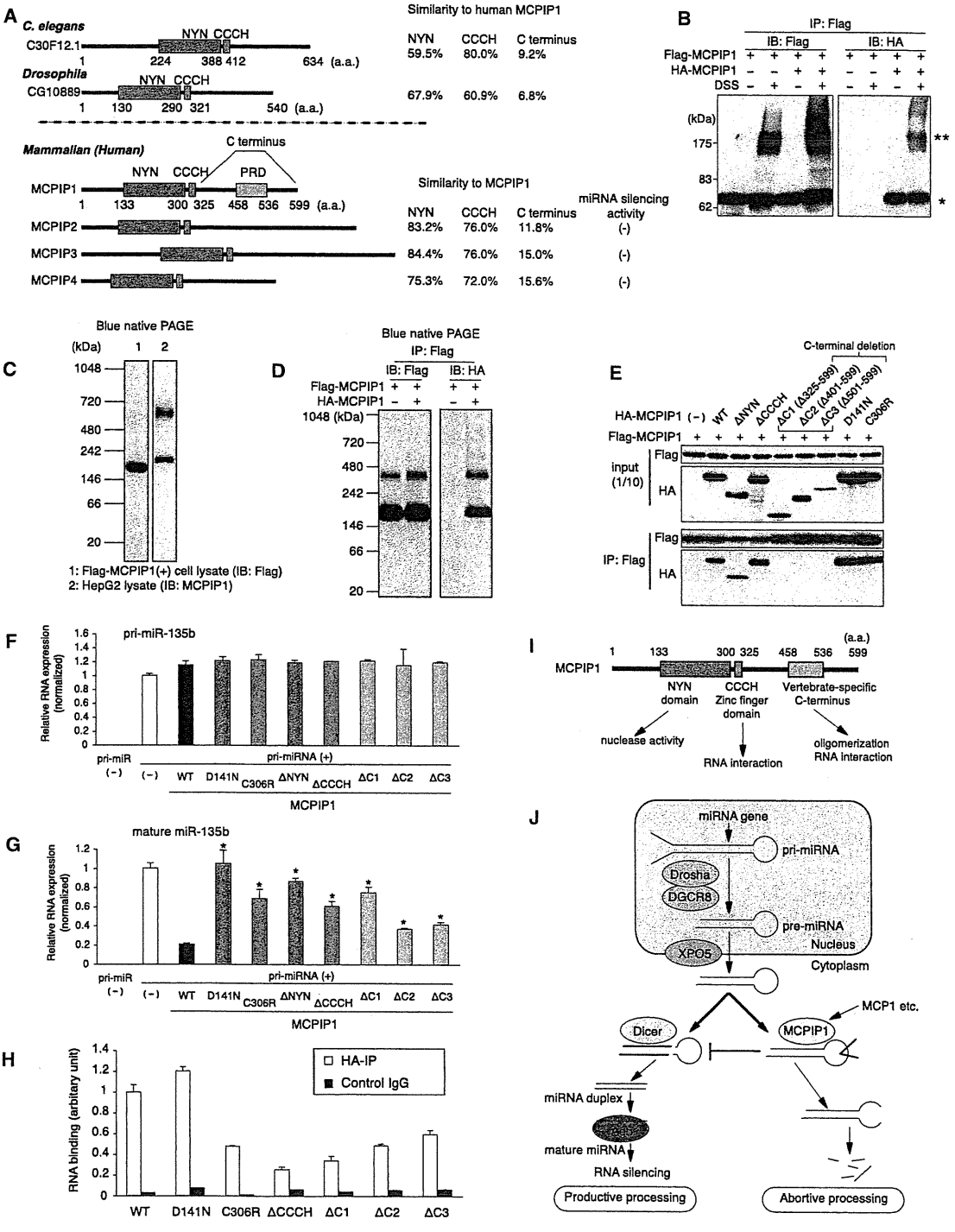

Figure 7. Oligomerization via Vertebrate-Specific C Terminus Is Important for miRNA Silencing Activity of MCPIP1

(A) Schematic representation of human MCPIP family proteins and invertebrate MCPIP1-related proteins (*C. elegans* C30F12.1 and *Drosophila* CG10889). The numbers on the right indicate the sequence similarity to human MCPIP1 protein.

(B) Oligomerization of MCPIP1. FLAG-MCPIP1 and HA-MCPIP1 were ectopically expressed in HEK293T cells. Cell lysates were crosslinked with DSS and immunoprecipitated with the anti-FLAG antibody followed by immunoblotting. Asterisks (*, **) indicate MCPIP1 monomers and oligomers, respectively.

physiological and pathological processes, such as inflammation and cancer.

EXPERIMENTAL PROCEDURES

Cell Lines, Antibodies, and Reagents

HEK293T, HepG2, Jurkat, and THP-1 cell lines were obtained from the American Type Culture Collection. HEK293T and HepG2 cells were maintained in Dulbecco's modified Eagle's medium (GIBCO) containing 10% fetal bovine serum (FBS). Hematological cell lines were maintained in RPMI1640 medium (GIBCO) with 10% FBS. Plasmids, antibodies, and reagents are described in the Supplemental Experimental Procedures.

Luciferase Reporter Assay, qRT-PCR Assays, and Northern Blot Analyses

Dual renilla/luciferase assays, qRT-PCR assays, and northern blot analyses were carried out as previously described (Suzuki et al., 2009). The expression levels of mature miRNAs were determined using TaqMan MicroRNA assay kit (Applied Biosystems) according to the manufacturer's protocol. The primer sequences used and related procedures are described in the Supplemental Experimental Procedures.

Immunocytochemistry

Immunostaining was carried out with anti-HA antibody, followed by counterstaining with TOTO-3 (Invitrogen–Molecular Probes). Stained specimens were examined using a LSM 510 META confocal microscope (Carl Zeiss).

In Vitro Pre-miRNA Cleavage Assay

In vitro pre-miRNA cleavage assay was performed modifying the method of in vitro pri-miRNA processing assay described previously (Suzuki et al., 2009). α^{32}P-UTP-internally-labeled pre-miRNAs were generated by in vitro transcription using PCR fragments containing pre-miRNA sequences fused to a T7 RNA polymerase promoter as templates. The detailed procedures are described in the Supplemental Experimental Procedures.

Immunoprecipitation and Immunoblot assay

Cells were lysed with Nonidet P-40 lysis buffer and subjected to immunoblot assay with standard procedures.

Cloning of Pre-miRNA Fragments

MCPIP1-cleaved RNA fragments were cloned and sequenced using microRNA cloning kit (Wako) according to the manufacturer's instructions. Briefly, the fragments were isolated using Trizol (Invitrogen), after in vitro cleavage reaction (90 min) without radioisotope as described above. We ligated 3′ adaptors into the RNA fragments with thermostable ssDNA ligase (Wako). The ligated substrate was reverse-transcribed, ligated with 5′ adaptors, and further PCR-amplified using HOT Goldstar DNA Polymerase (Wako). The PCR products were cloned into pCR2.1-TOPO vectors (Invitrogen) and sequenced.

RNA Immunoprecipitation Assay

RNA immunoprecipitation assay was performed as previously described (Suzuki et al., 2009).

Gene Expression Profiling Analysis

Gene expression profiling data of lung cancer patients were previously described (in Bild et al., 2006 [Figures 4C–4E], Shedden et al., 2008 [Figures S4B and S4D], and Larsen et al., 2007 [Figures S4C and S4E]), and were obtained from caArray system or NCBI's Gene Expression Omnibus. The expression levels of Dicer or MCPIP1 were evaluated by the corresponding probes. GSEA was performed with GSEA software available from the Broad Institute (http://www.broadinstitute.org/gsea/) (Subramanian et al., 2005). GSEA-embedded potential miRNA target gene sets were used. Survival analysis was performed using the survival package of R, the survfit function and the survdiff function.

SUPPLEMENTAL INFORMATION

Supplemental Information includes seven figures and Supplemental Experimental Procedures and can be found with this article online at doi:10.1016/j.molcel.2011.09.012.

ACKNOWLEDGMENTS

We thank K. Isogaya, K. Horiguchi, D. Koinuma, and T. Watabe for discussion; M. Tanaka and T. Funakoshi (Wako) for technical advice; T. Yokochi for encouragement; and all members of the Department of Molecular Pathology, at the University of Tokyo. This work was supported by KAKENHI (Grant-in-Aid for Scientific Research for Research Activity start-up [No. 22890038] and on Innovative Areas "RNA regulation" [No. 23112702]), the Global Center of Excellence Program for "Integrative Life Science Based on the Study of Biosignaling Mechanisms" from the Ministry of Education, Culture, Sports, Science, and Technology of Japan, and the Cell Science Research Foundation.

Received: March 4, 2011
Revised: June 17, 2011
Accepted: September 7, 2011
Published: November 3, 2011

REFERENCES

Anantharaman, V., and Aravind, L. (2006). The NYN domains: novel predicted RNAses with a PIN domain-like fold. RNA Biol. *3*, 18–27.

Bergdoll, M., Remy, M.H., Cagnon, C., Masson, J.M., and Dumas, P. (1997). Proline-dependent oligomerization with arm exchange. Structure *5*, 391–401.

Bild, A.H., Yao, G., Chang, J.T., Wang, Q., Potti, A., Chasse, D., Joshi, M.B., Harpole, D., Lancaster, J.M., Berchuck, A., et al. (2006). Oncogenic pathway signatures in human cancers as a guide to targeted therapies. Nature *439*, 353–357.

Chatterjee, S., and Grosshans, H. (2009). Active turnover modulates mature microRNA activity in Caenorhabditis elegans. Nature *461*, 546–549.

(C and D) Blue native PAGE analyses. HEK293T cells expressing FLAG-MCPIP1 or HepG2 cells were subjected to blue native PAGE analysis using FLAG antibody or MCPIP1 antibody (C). FLAG immunoprecipitates from cell lysates containing FLAG-MCPIP1 and HA-MCPIP1 were also analyzed by blue native PAGE analysis after elution with FLAG peptide (D).

(E) Requirement of the C terminus for MCPIP1 oligomerization. FLAG-MCPIP1 and HA-MCPIP1 mutants were ectopically expressed in HEK293T cells. Cell lysates were immunoprecipitated with the anti-FLAG antibody followed by immunoblotting.

(F and G) Effects of MCPIP1 mutation on miRNA maturation. MCPIP1 mutants were coexpressed with pri-miR-135b in HEK293T cells. At 48 hr posttransfection, the expression levels of pri-miRNA (F) and mature miRNA (G) were analyzed with qRT-PCR analyses (*$p < 0.05$, compared to wild-type MCPIP1 [WT]; n = 3).

(H) pre-miRNA binding capacity of MCPIP1 mutants. HEK293T cells were cotransfected with pri-miR-135b expression vector and various MCPIP1 mutant expression vectors. After transfection, MCPIP1 mutants were immunoprecipitated with anti-HA antibody and subjected to RT-PCR analysis with pre-miR-135b primers. As controls, RNA samples immunoprecipitated with nonspecific IgG (Control IgG; n = 3) were subjected to PCR.

(I) Differential contribution of MCPIP1 domains for miRNA silencing activity.

(J) A schematic model for the inhibition of miRNA processing by MCPIP1. See also Figure S7. Error bars represent SEM.

Costinean, S., Sandhu, S.K., Pedersen, I.M., Tili, E., Trotta, R., Perrotti, D., Ciarlariello, D., Neviani, P., Harb, J., Kauffman, L.R., et al. (2009). Src homology 2 domain-containing inositol-5-phosphatase and CCAAT enhancer-binding protein beta are targeted by miR-155 in B cells of Emicro-MiR-155 transgenic mice. Blood *114*, 1374–1382.

Davis, B.N., and Hata, A. (2009). Regulation of MicroRNA Biogenesis: A miRiad of mechanisms. Cell Commun. Signal. *7*, 18.

Han, J., Pedersen, J.S., Kwon, S.C., Belair, C.D., Kim, Y.K., Yeom, K.H., Yang, W.Y., Haussler, D., Blelloch, R., and Kim, V.N. (2009). Posttranscriptional crossregulation between Drosha and DGCR8. Cell *136*, 75–84.

Heo, I., Joo, C., Cho, J., Ha, M., Han, J., and Kim, V.N. (2008). Lin28 mediates the terminal uridylation of let-7 precursor MicroRNA. Mol. Cell *32*, 276–284.

Karube, Y., Tanaka, H., Osada, H., Tomida, S., Tatematsu, Y., Yanagisawa, K., Yatabe, Y., Takamizawa, J., Miyoshi, S., Mitsudomi, T., and Takahashi, T. (2005). Reduced expression of Dicer associated with poor prognosis in lung cancer patients. Cancer Sci. *96*, 111–115.

Kumar, M.S., Lu, J., Mercer, K.L., Golub, T.R., and Jacks, T. (2007). Impaired microRNA processing enhances cellular transformation and tumorigenesis. Nat. Genet. *39*, 673–677.

Larsen, J.E., Pavey, S.J., Passmore, L.H., Bowman, R., Clarke, B.E., Hayward, N.K., and Fong, K.M. (2007). Expression profiling defines a recurrence signature in lung squamous cell carcinoma. Carcinogenesis *28*, 760–766.

Li, T., Morgan, M.J., Choksi, S., Zhang, Y., Kim, Y.S., and Liu, Z.G. (2010). MicroRNAs modulate the noncanonical transcription factor NF-kappaB pathway by regulating expression of the kinase IKKalpha during macrophage differentiation. Nat. Immunol. *11*, 799–805.

Liang, J., Song, W., Tromp, G., Kolattukudy, P.E., and Fu, M. (2008a). Genome-wide survey and expression profiling of CCCH-zinc finger family reveals a functional module in macrophage activation. PLoS ONE *3*, e2880.

Liang, J., Wang, J., Azfer, A., Song, W., Tromp, G., Kolattukudy, P.E., and Fu, M. (2008b). A novel CCCH-zinc finger protein family regulates proinflammatory activation of macrophages. J. Biol. Chem. *283*, 6337–6346.

Lu, J., Getz, G., Miska, E.A., Alvarez-Saavedra, E., Lamb, J., Peck, D., Sweet-Cordero, A., Ebert, B.L., Mak, R.H., Ferrando, A.A., et al. (2005). MicroRNA expression profiles classify human cancers. Nature *435*, 834–838.

Martello, G., Rosato, A., Ferrari, F., Manfrin, A., Cordenonsi, M., Dupont, S., Enzo, E., Guzzardo, V., Rondina, M., Spruce, T., et al. (2010). A MicroRNA targeting dicer for metastasis control. Cell *141*, 1195–1207.

Matsushita, K., Takeuchi, O., Standley, D.M., Kumagai, Y., Kawagoe, T., Miyake, T., Satoh, T., Kato, H., Tsujimura, T., Nakamura, H., and Akira, S. (2009). Zc3h12a is an RNase essential for controlling immune responses by regulating mRNA decay. Nature *458*, 1185–1190.

Melo, S.A., Moutinho, C., Ropero, S., Calin, G.A., Rossi, S., Spizzo, R., Fernandez, A.F., Davalos, V., Villanueva, A., Montoya, G., et al. (2010). A genetic defect in exportin-5 traps precursor microRNAs in the nucleus of cancer cells. Cancer Cell *18*, 303–315.

Merritt, W.M., Lin, Y.G., Han, L.Y., Kamat, A.A., Spannuth, W.A., Schmandt, R., Urbauer, D., Pennacchio, L.A., Cheng, J.F., Nick, A.M., et al. (2008). Dicer, Drosha, and outcomes in patients with ovarian cancer. N. Engl. J. Med. *359*, 2641–2650.

Moschos, S.A., Williams, A.E., Perry, M.M., Birrell, M.A., Belvisi, M.G., and Lindsay, M.A. (2007). Expression profiling in vivo demonstrates rapid changes in lung microRNA levels following lipopolysaccharide-induced inflammation but not in the anti-inflammatory action of glucocorticoids. BMC Genomics *8*, 240.

Nagel, R., le Sage, C., Diosdado, B., van der Waal, M., Oude Vrielink, J.A., Bolijn, A., Meijer, G.A., and Agami, R. (2008). Regulation of the adenomatous polyposis coli gene by the miR-135 family in colorectal cancer. Cancer Res. *68*, 5795–5802.

O'Connell, R.M., Rao, D.S., Chaudhuri, A.A., and Baltimore, D. (2010). Physiological and pathological roles for microRNAs in the immune system. Nat. Rev. Immunol. *10*, 111–122.

Ozen, M., Creighton, C.J., Ozdemir, M., and Ittmann, M. (2008). Widespread deregulation of microRNA expression in human prostate cancer. Oncogene *27*, 1788–1793.

Paschoud, S., Dogar, A.M., Kuntz, C., Grisoni-Neupert, B., Richman, L., and Kühn, L.C. (2006). Destabilization of interleukin-6 mRNA requires a putative RNA stem-loop structure, an AU-rich element, and the RNA-binding protein AUF1. Mol. Cell. Biol. *26*, 8228–8241.

Ramachandran, V., and Chen, X. (2008). Degradation of microRNAs by a family of exoribonucleases in Arabidopsis. Science *321*, 1490–1492.

Rodriguez, A., Vigorito, E., Clare, S., Warren, M.V., Couttet, P., Soond, D.R., van Dongen, S., Grocock, R.J., Das, P.P., Miska, E.A., et al. (2007). Requirement of bic/microRNA-155 for normal immune function. Science *316*, 608–611.

Ruggiero, T., Trabucchi, M., De Santa, F., Zupo, S., Harfe, B.D., McManus, M.T., Rosenfeld, M.G., Briata, P., and Gherzi, R. (2009). LPS induces KH-type splicing regulatory protein-dependent processing of microRNA-155 precursors in macrophages. FASEB J. *23*, 2898–2908.

Sadler, A.J., and Williams, B.R. (2008). Interferon-inducible antiviral effectors. Nat. Rev. Immunol. *8*, 559–568.

Salehzada, T., Silhol, M., Steff, A.M., Lebleu, B., and Bisbal, C. (1993). 2′,5′-Oligoadenylate-dependent RNase L is a dimer of regulatory and catalytic subunits. J. Biol. Chem. *268*, 7733–7740.

Sandberg, R., Neilson, J.R., Sarma, A., Sharp, P.A., and Burge, C.B. (2008). Proliferating cells express mRNAs with shortened 3′ untranslated regions and fewer microRNA target sites. Science *320*, 1643–1647.

Shedden, K., Taylor, J.M., Enkemann, S.A., Tsao, M.S., Yeatman, T.J., Gerald, W.L., Eschrich, S., Jurisica, I., Giordano, T.J., Misek, D.E., et al; Director's Challenge Consortium for the Molecular Classification of Lung Adenocarcinoma. (2008). Gene expression-based survival prediction in lung adenocarcinoma: a multi-site, blinded validation study. Nat. Med. *14*, 822–827.

Siomi, H., and Siomi, M.C. (2010). Posttranscriptional regulation of microRNA biogenesis in animals. Mol. Cell *38*, 323–332.

Subramanian, A., Tamayo, P., Mootha, V.K., Mukherjee, S., Ebert, B.L., Gillette, M.A., Paulovich, A., Pomeroy, S.L., Golub, T.R., Lander, E.S., and Mesirov, J.P. (2005). Gene set enrichment analysis: a knowledge-based approach for interpreting genome-wide expression profiles. Proc. Natl. Acad. Sci. USA *102*, 15545–15550.

Suzuki, H.I., and Miyazono, K. (2010). Dynamics of microRNA biogenesis: crosstalk between p53 network and microRNA processing pathway. J. Mol. Med. *88*, 1085–1094.

Suzuki, H.I., and Miyazono, K. (2011). Emerging complexity of microRNA generation cascades. J. Biochem. *149*, 15–25.

Suzuki, H.I., Yamagata, K., Sugimoto, K., Iwamoto, T., Kato, S., and Miyazono, K. (2009). Modulation of microRNA processing by p53. Nature *460*, 529–533.

Umbach, J.L., and Cullen, B.R. (2009). The role of RNAi and microRNAs in animal virus replication and antiviral immunity. Genes Dev. *23*, 1151–1164.

Wu, H., Neilson, J.R., Kumar, P., Manocha, M., Shankar, P., Sharp, P.A., and Manjunath, N. (2007). miRNA profiling of naïve, effector and memory CD8 T cells. PLoS ONE *2*, e1020.

Xiao, C., Srinivasan, L., Calado, D.P., Patterson, H.C., Zhang, B., Wang, J., Henderson, J.M., Kutok, J.L., and Rajewsky, K. (2008). Lymphoproliferative disease and autoimmunity in mice with increased miR-17-92 expression in lymphocytes. Nat. Immunol. *9*, 405–414.

Zhang, H., Kolb, F.A., Jaskiewicz, L., Westhof, E., and Filipowicz, W. (2004). Single processing center models for human Dicer and bacterial RNase III. Cell *118*, 57–68.

Zuker, M. (2003). Mfold web server for nucleic acid folding and hybridization prediction. Nucleic Acids Res. *31*, 3406–3415.

Overexpression of enhancer of zeste homolog 2 with trimethylation of lysine 27 on histone H3 in adult T-cell leukemia/lymphoma as a target for epigenetic therapy

Daisuke Sasaki,[1] Yoshitaka Imaizumi,[2] Hiroo Hasegawa,[1] Akemi Osaka,[1] Kunihiro Tsukasaki,[2] Young Lim Choi,[3] Hiroyuki Mano,[3] Victor E. Marquez,[4] Tomayoshi Hayashi,[5] Katsunori Yanagihara,[1] Yuji Moriwaki,[2] Yasushi Miyazaki,[2] Shimeru Kamihira,[1] and Yasuaki Yamada[1]

[1]Department of Laboratory Medicine, Nagasaki University Graduate School of Biomedical Sciences, Nagasaki, Japan; [2]Department of Hematology and Molecular Medicine, Atomic Bomb Disease Institute, Nagasaki University Graduate School of Biomedical Sciences, Nagasaki, Japan; [3]Division of Functional Genomics, Jichi Medical University, Tochigi, Japan; [4]Chemical Biology Laboratory, National Cancer Institute, Frederick, MD, USA; and [5]Department of Pathology, Nagasaki University Hospital, Nagasaki, Japan

ABSTRACT

Background
Enhancer of zeste homolog 2 is a component of the Polycomb repressive complex 2 that mediates chromatin-based gene silencing through trimethylation of lysine 27 on histone H3. This complex plays vital roles in the regulation of development-specific gene expression.

Design and Methods
In this study, a comparative microarray analysis of gene expression in primary adult T-cell leukemia/lymphoma samples was performed, and the results were evaluated for their oncogenic and clinical significance.

Results
Significantly higher levels of Enhancr of zeste homolog 2 and RING1 and YY1 binding protein transcripts with enhanced levels of trimethylation of lysine 27 on histone H3 were found in adult T-cell leukemia/lymphoma cells compared with those in normal CD4$^+$ T cells. Furthermore, there was an inverse correlation between the expression level of Enhancer of zeste homolog 2 and that of miR-101 or miR-128a, suggesting that the altered expression of the latter miRNAs accounts for the overexpression of the former. Patients with high Enhancer of zeste homolog 2 or RING1 and YY1 binding protein transcripts had a significantly worse prognosis than those without it, indicating a possible role of these genes in the oncogenesis and progression of this disease. Indeed, adult T-cell leukemia/lymphoma cells were sensitive to a histone methylation inhibitor, 3-deazaneplanocin A. Furthermore, 3-deazaneplanocin A and histone deacetylase inhibitor panobinostat showed a synergistic effect in killing the cells

Conclusions
These findings reveal that adult T-cell leukemia/lymphoma cells have deregulated Polycomb repressive complex 2 with over-expressed Enhancer of zeste homolog 2, and that there is the possibility of a new therapeutic strategy targeting histone methylation in this disease.

Key words: adult T-cell leukemia/lymphoma, human T-cell leukemia virus type-1, Enhancer of zeste homolog 2, H3K27me3.

Citation: Sasaki D, Imaizumi Y, Hasegawa H, Osaka A, Tsukasaki K, Choi YL, Mano H, Marquez VE, Hayashi T, Yanagihara K, Moriwaki Y, Miyazaki Y, Kamihira S, and Yamada Y. Overexpression of enhancer of zeste homolog 2 with trimethylation of lysine 27 on histone H3 in adult T-cell leukemia/lymphoma as a target for epigenetic therapy Haematologica 2011;96(4):712-719. doi:10.3324/haematol.2010.028605

©2011 Ferrata Storti Foundation. This is an open-access paper.

Funding: supported in part by a Grant-in-Aid for Scientific Research from the Ministry of Health, Labour, and Welfare of Japan (N. 04010119). For VEM, this research was supported in part by the Intramural Research Program of the NIH, Center for Cancer Research, NCI-Frederick.

Acknowledgments: the authors thank Sayaka Mori and Yuko Doi for excellent technical assistance.

Manuscript received June 16, 2010. Revised version arrived on December 16, 2010. Manuscript accepted on December 31, 2010.

Correspondence:
Yasuaki Yamada, Department of Laboratory Medicine, 1-7-1 Sakamoto, Nagasaki 852-8501, Japan. Phone: international +81.958197408.
Fax: international +81.958197422.
E-mail: y-yamada@nagasaki-u.ac.jp

The online version of this article has a Supplementary Appendix.

Introduction

The Polycomb group (PcG) proteins play critical roles in the regulation of development by repressing specific sets of developmental genes through chromatin modification.[1] They form two distinct multimeric complexes, Polycomb repressive complex 1 (PRC1) and PRC2, which bind to polycomb responsive elements (PRE), repress genes required for cell differentiation, and maintain pluripotency and self-renewal of embryonic stem cells and hematopoietic stem cells.[2,3] PRC2 consists of Enhancer of zeste homolog 2 (EZH2), which has histone methyltransferase activity, suppressor of zeste 12 (SUZ12), and embryonic ectoderm development (EED), which is required to maintain the integrity of PRC2.[1,4] Sequence-specific DNA binding protein YY1, which recognizes PRE, interacts with EED and recruits PRC2 to a specific chromatin domain to be repressed.[5] EED interacts with histone deacetylase (HDAC) proteins, HDAC1 and HDAC2, and the histone binding proteins RBBP4 (RbAp48) and RBBP7 (RbAp46).[6] PRC2 thus also participates in histone deacetylation. EZH2, as a part of the PRC2 complex, not only methylates histone but also serves as a recruitment platform for DNA methyltransferases that methylate the promoter regions of target genes, which is another mechanism of gene repression.[7] The more diverse complex PRC1 consists of HPC family proteins that mediate chromatin association, HPH family proteins, RING, BMI1, and others.[1] PRC2 initiates trimethylation of lysine 27 on histone H3 (H3K27me3) and, to a lesser extent, lysine 9 of histone H3.[8] PRC1 recognizes H3K27me3 through the chromodomain of the HPC and maintains the trimethylation. There are a number of reports indicating that such epigenetically mediated transcriptional silencing is associated with cancer development.[1,9] Among these, oncogenic roles of over-expressed EZH2 have been studied in a variety of tumors.[10]

Adult T-cell leukemia/lymphoma (ATL) is a neoplasm of mature CD4+ T-cell origin, etiologically associated with human T-cell leukemia virus type-1 (HTLV-1).[11,12] Its clinical behavior differs among patients and is subclassified into four subtypes: smoldering type and chronic type as indolent subtypes, and acute type and lymphoma type as aggressive subtypes.[13] Inactivation of tumor suppressor genes is one of the key events in development and progression, and there is a strong accumulation of *p14ARF/p15INK4B/p16INK4A* gene deletion/methylation or *p53* gene mutations in aggressive subtypes (>60%).[14-20] In the present study, for further investigation of the oncogenesis of ATL, we performed a comparative microarray analysis of gene expression in primary ATL samples. ATL cells expressed significantly higher levels of *EZH2* and *RYBP* (RING1 and YY1 binding protein) transcripts than CD4+ T cells from healthy volunteers. Moreover, acute-type ATL cells showed significantly higher levels of these transcripts than chronic-type ATL cells, suggesting that deregulation of PcG proteins plays a crucial role not only in the development but also in the progression of ATL. In addition, ATL samples were strongly positive for H3K27me3, and were sensitive to 3-deazaneplanocin A (DZNep), a histone methylation inhibitor.[21-23] It has recently been shown that HDAC inhibitor panobinostat (PS, also known as LBH589) depletes the levels of EZH2, SUZ12, and EED and induces apoptotic death in leukemia cells.[24] Deregulation of PcG protein genes with over-expressed EZH2 in ATL cells suggests that ATL is one of the appropriate target diseases for such epigenetic therapy.

Design and Methods

Sample preparation

This study was approved by the ethics committees of Nagasaki University, and all clinical samples were obtained after written informed consent was provided. The diagnosis of ATL was confirmed by the monoclonal integration of HTLV-1 proviral DNA in the genomic DNA of leukemia cells. Peripheral blood mononuclear cells (PBMCs) were obtained from ATL patients (acute type 22 cases, chronic type 19 cases) and healthy adult volunteers by density gradient centrifugation using Lympho-prep (AXIS SHIELD, Oslo, Norway). For enrichment of ATL cells, CD4+ cells were purified from the PBMCs by the magnetic bead method (CD4 MicroBeads, Miltenyi Biotec, Auburn, CA, USA) as described elsewhere.[25] Besides these samples for microarray analysis, we prepared another set of samples for quantitative real-time RT-PCR (qRT-PCR) and Western blotting (25 ATL patients, 13 HTLV-1 carriers, and 12 healthy adults) to confirm the results of microarray analysis. We also used formalin-fixed, paraffin-embedded lymph nodes from 7 patients with lymphoma-type ATL and 5 patients with follicular lymphoma for immunohistochemical analysis.

ATL cell lines used in this study, SO4, ST1, KK1, KOB, and LM-Y1, were established from respective patients in our laboratory and have been confirmed to be of primary ATL cell origin.[26] Cells were maintained in RPMI1640 medium supplemented with 10% FBS and 100 Japan reference units of recombinant interleukin-2 (rIL-2) (kindly provided by Takeda Pharmaceutical Company, Ltd., Osaka, Japan). We also used HTLV-1-infected T-cell lines MT2 and HuT102 and acute T-lymphoblastic leukemia cell lines Jurkat and MOLT4, which were maintained without rIL-2.

DNA microarray analysis

RNA was prepared from purified CD4+ T cells, and subjected to hybridization to HGU133A & B microarray containing 44,760 probe sets for human genes (Affymetrix, Santa Clara, CA, USA) as described previously.[25,27] The mean expression intensity of the internal positive control probe sets (*http://www.affymetrix.com/support/technical/mask_files.affx*) was set to 500 units in each hybridization, and the fluorescence intensity of each test gene was normalized accordingly. All HGU133A & B microarray data are available from the Gene Expression Omnibus website (*http://www.ncbi.nlm.nih.gov/geo*) under the accession number GSE1466.

Quantitative real-time RT-PCR

For confirmation of the results of microarray analysis, we performed quantitative real-time RT-PCR (qRT-PCR) for PcG protein genes. Total RNA was prepared using Isogen (Wako, Osaka, Japan). After removal of contaminated DNA with DNase (Message Clean kit; GenHunter, Nashville, TN, USA), cDNA was constructed from 1 μg of total RNA using the SuperScript III RT-PCR System (Invitrogen, Carlsbad, CA, USA) according to the manufacturer's instructions. Primers and TaqMan probes labeled with TAMRA dye at the 3' end and FAM at the 5' end are listed in *Online Supplementary Table S1*. The mRNA levels for PcG family proteins and porphobilinogen deaminase (PBGD) were measured from a cDNA template using a LightCycler480 PCR System (Roche Diagnostics, Mannheim, Germany). Briefly, reactions were performed in a 20 μL volume with 5 μL (25 ng) of cDNA, 0.5 μM PCR primers, 0.1 μM TaqMan probes, and 10 μL of LightCycler

480 probes Master Mix (Roche Diagnostics). The PCR program consisted of 95°C for 5 min followed by 50 cycles of 95°C for 10 sec and 60°C for 30 sec. After 50 cycles, the absolute amounts of PcG protein mRNA and *PBGD* mRNA were interpolated from the standard curves generated by the dilution method using plasmids derived from a clone transfected with pTAC-1 Vector (BioDynamics Laboratory Inc., Tokyo, Japan) containing amplicons from the PcG family protein and PBGD genes, respectively. To normalize these results for variability in concentration and integrity of RNA and cDNA, the *PBGD* gene was used as an internal control in each sample.

For the quantitative PCR for microRNAs (miRNAs), miR-101, miR-26a, and miR-128a, 10 ng of total RNA (containing miRNA) was used. RT reaction and real-time quantification were performed using TaqMan MicroRNA RT kit and TaqMan MicroRNA assays (hsa-miR-26a, assay ID 000405; hsa-miR-101, assay ID 002253; hsa-miR-128a, assay ID 002216; RNU6B, assay ID 001093) (Applied Biosystems, Foster City, CA, USA) in accordance with the manufacturer's instructions. Each PCR reaction mixture contained 10 μL of LightCycler 480 probes Master Mix, 4 μL of nuclease-free water, 1 μL of 20X specific PCR primer, and 5 μL of RT product. The thermal cycler was programmed as follows: 95°C for 5 min, 40 cycles of 95°C for 15 sec, and 60°C for 60 sec. Using the comparative CT method, we used an endogenous control (RNU6B) to normalize the expression levels of target micro-RNA by correcting differences in the amount of RNA loaded into qPCR reactions.

Western blot analysis and antibodies

Western blot analysis was performed as described previously.[28] The analysis was performed using antibodies to EZH2 and Histone H3 (Cell Signaling Technology, Danvers, MA, USA), phospho EZH2 (Ser21) (Bethyl Laboratories, Montgomery, TX, USA), H3K27me3, dimethylated H3K27 (H3K27me2), monomethylated H3K27 (H3K27me1) (Millipore, Temecula, CA, USA), and β-actin (Sigma, St. Louis, MO, USA).

Immunohistochemistry

Immunohistochemical staining for EZH2 and H3K27me3 was performed on formalin-fixed, paraffin-embedded lymph node samples from lymphoma-type ATL patients and follicular lymphoma patients as a control. The deparaffinized slides were pretreated with DAKO Target Retrieval Solution, pH 9 (DAKO Japan, Tokyo, Japan), and heated in a water bath at 95°C for 40 min. For all stains, the endogenous peroxidase was quenched using 3% H_2O_2 for 15 min. Sections were then placed in 0.5% non-fat dry milk for 30 min at room temperature. The primary antibodies used were anti-EZH2 antibody (BD Biosciences, San Jose, CA, USA) and anti-H3K27me3 antibody (Cell Signaling Technology, Boston, MA, USA), and were applied at 1:50 dilution and 1:100 dilution, respectively. They were allowed to react for 1 h at room temperature, and then the DAKO EnVision™ + Dual Link System-HRP (DAKO Japan, Tokyo, Japan) was applied using diaminobenzidine as the chromogen, following the manufacturer's protocol.

Sensitivity of adult T-cell leukemia/lymphoma cell lines to DZNep and PS (LBH589)

DZNep was synthesized by one of the authors (VEM). Cells were treated with different concentrations of DZNep for 72 h and the cell proliferation status was evaluated by an MTS assay using a Cell Titer 96® AQueos Cell Proliferation Assay kit (Promega, Madison, WI, USA) in accordance with the manufacturer's instructions. To analyze the synergistic effect of combined treatment with DZNep and PS (LBH589) (kindly provided by Novartis Pharma AG, Basel, Switzerland), cells were treated with DZNep (0.3-5.0 μM) and PS (LBH589) (3-50 nM) for 48 h. After the cell proliferation status was evaluated by an MTS assay, the combination index (CI) for each drug combination was obtained by determining the median dose effect of Chou and Talalay using the CI equation within the commercially available software Calcusyn (Biosoft).[29] CI<1, CI=1, and CI>1 indicate synergism, additive effect, and antagonism, respectively. Cell viability represents the value relative to that of the control culture without these agents.

Results

Microarray analysis shows increased EZH2 and/or RYBP transcripts in adult T-cell leukemia/lymphoma cells

In a comparative microarray analysis of primary ATL samples, we focused on investigating PcG protein genes, *EZH2*, *RYBP*, *BMI-1*, and *CBX7*, in the present study because ATL cells show many aberrantly hypermethylated DNA sequences.[30] ATL cells expressed significantly higher levels of *EZH2* and *RYBP* transcripts than $CD4^+$ T cells from healthy adults (Figure 1A and B). In addition, there was a difference between ATL subtypes in these expressions, and cells from the acute type showed significantly higher levels of these transcripts than the cells from the chronic type. When patients were separated into two groups consisting of those with high expression and those with low expression, the group with high *EZH2* or high *RYBP* transcript showed significantly shorter survival than the respective low-expression groups (Figure 1E and F), indicating that high *EZH2* and/or *RYBP* expression is associated with aggressive clinical behavior. Convincingly, there was a trend toward accumulation of acute-type ATL in the high *EZH2* or the high *RYBP* expression group: 14 cases of acute type and 6 cases of chronic type in the high *EZH2* group, 7 cases of acute type and 13 cases of chronic type in the low *EZH2* group, 14 cases of acute type and 6 cases of chronic type in the high RYBP group, and 7 cases of acute type and 13 cases of chronic type in the low RYBP group. BMI1 is known to down-regulate the expression of *p14ARF/p16INK4A* and lead to neoplastic transformation.[31] Chromobox 7 (CBX7), a component of the PRC1, is also known to repress the transcription of *p14ARF/p16INK4A*.[32] Since inactivation of *p14ARF/p15INK4B/p16INK4A* genes is one of the key events in ATL progression, expression of *BMI-1* and/or *CBX7* transcript was expected to be elevated in acute-type ATL cells. There was, however, no difference in these expressions between ATL subtypes or even between ATL cells and normal $CD4^+$ T cells (Figure 1C and D). There was no difference in survival for different *BMI-1* or *CBX7* expression levels (Figure 1G and H).

Confirmation of increased EZH2 and/or RYBP transcripts by quantitative real-time RT-PCR

For confirmation of the results of microarray analysis, we quantified the transcripts of the PcG protein genes including *EZH2* and *RYBP* by qRT-PCR using another set of samples from ATL patients, healthy adults, HTLV-1 carriers, and hematologic cell lines including ATL cell lines. In accordance with the results of microarray analysis, *EZH2* and *RYBP* transcripts were increased in primary ATL cells compared with those in the cells from healthy adults and HTLV-1 carriers, with statistically significantly higher val-

ues in *EZH2* in terms of both absolute copy number per 25 ng of total RNA and normalized expression level (*Online Supplementary Figure S1A, a, B, b*). *RBBP4* was significantly higher in primary ATL cells than in the cells from healthy adults and HTLV-1 carriers in terms of normalized expression level (*Online Supplementary Figure S1 C, c*). In contrast, there was no difference in *BMI1*, *YY1*, and *EED* expressions among these groups, although some patients showed very high *BMI1* expression (*Online Supplementary Figure S1D, d, E, e, F, f*). Similarly to primary ATL cells, some ATL cell lines showed high *EZH2* expression in terms of absolute copy number per 25 ng of total RNA (*Online Supplementary Figure S1A*).

EZH2 protein expression with trimethylation of H3K27 is characteristic in adult T-cell leukemia/lymphoma cells

We then examined EZH2 and RYBP at the protein level by Western blotting. A 98-kDa band for EZH2 protein and a 32-kDa band for RYBP protein were detected in all primary ATL samples irrespective of subtype, but they were hardly detected in cells from healthy adults and HTLV-1 carriers (Figure 2A, *Online Supplementary Figure S2*, and *data not shown*). ATL cell lines and acute T-lymphoblastic leukemia cell lines also showed intense EZH2 bands. The serine-threonine kinase Akt phosphorylates EZH2 at serine 21 and suppresses its methyltransferase activity by impeding EZH2 binding to histone H3, which results in a decrease in lysine 27 trimethylation.[33] EZH2 of ATL cells was not phosphorylated and was in its active form (Figure 2A). In fact, most primary ATL samples showed the band for H3K27me3, while the cells from healthy adults lacked the band (Figure 2B). As it is known that EZH2 plays a crucial role in trimethylation but not in dimethylation or monomethylation, the bands for H3K27me2 and H3K27me1 were detected in all samples examined, but the band for H3K27me3 was limited in primary ATL cells and ATL cell lines LMY1 and KOB that showed an intense EZH2 band with a faint phosphorylated EZH2 band (Figure 2A and B). In contrast, EZH2 was strongly phosphorylated in ATL cell lines ST1, SO4, KK1, and acute T-lymphoblastic leukemia cell lines Jurkat and MOLT4, and these cell lines hardly showed the band for H3K27me3. Collectively, these results indicate that ATL cells express

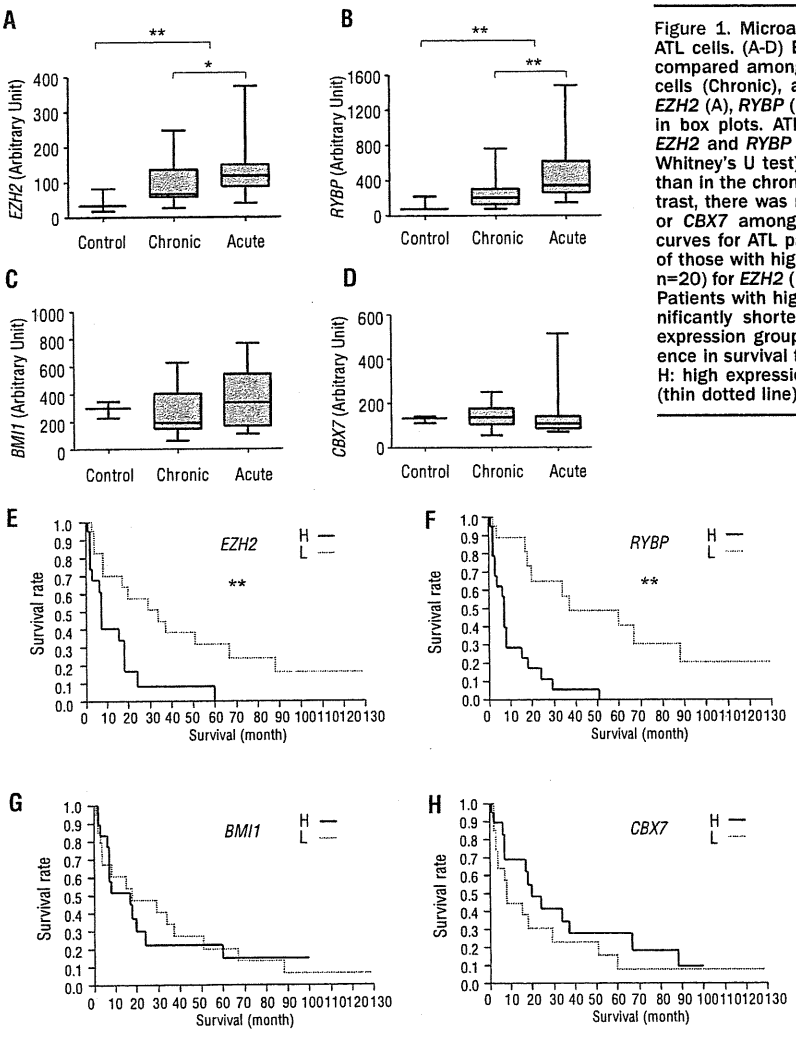

Figure 1. Microarray analysis of gene expression in primary ATL cells. (A-D) Expression levels of PcG protein genes were compared among normal CD4⁺ T cells (Control), chronic ATL cells (Chronic), and acute ATL cells (Acute), and results of *EZH2* (A), *RYBP* (B), *BMI1* (C), and *CBX7* (D) are demonstrated in box plots. ATL cells showed significantly higher levels of *EZH2* and *RYBP* transcripts than normal CD4⁺ T cells (Mann-Whitney's U test), with a higher expression in the acute type than in the chronic type (Mann-Whitney's U test) (A, B). In contrast, there was no statistical difference in the level for *BMI1* or *CBX7* among these groups (C, D). (E-H) Overall survival curves for ATL patients separated into two groups consisting of those with high expression (H, n=20) and low expression (L, n=20) for *EZH2* (E), *RYBP* (F), *BMI1* (G), or *CBX7* (H) are shown. Patients with high *EZH2* or high *RYBP* expression showed significantly shorter survival than those in corresponding low expression groups (log rank test) (E, F). There was no difference in survival for different *BMI1* or *CBX7* expressions (G, H). H: high expression group (bold line), L: low expression group (thin dotted line). *P<0.05, **P<0.01

functionally active EZH2, and as a result, their H3K27 are trimethylated, and that ATL cell lines LMY1 and KOB preserve this characteristic of primary ATL cells.

Immunohistochemical confirmation of the expression of EZH2 and H3K27me3 in lymph nodes

We next used lymph nodes from lymphoma-type ATL patients for immunohistochemical evaluation of EZH2 expression and H3K27me3. In agreement with the results of Western blotting, all ATL lymph nodes from 7 patients were strongly positive for both EZH2 and H3K27me3 without exception in their nuclear staining (*Online Supplementary Figure S3* and *data not shown*), suggesting that overexpression of EZH2 with H3K27me3 is a common feature of ATL cells irrespective of ATL subtypes. In contrast, in lymph nodes from 5 follicular lymphoma patients, only a few cells were positive for EZH2 with some variation among patients and most cells were negative for H3K27me3 (*Online Supplementary Figure S3* and *data not shown*).

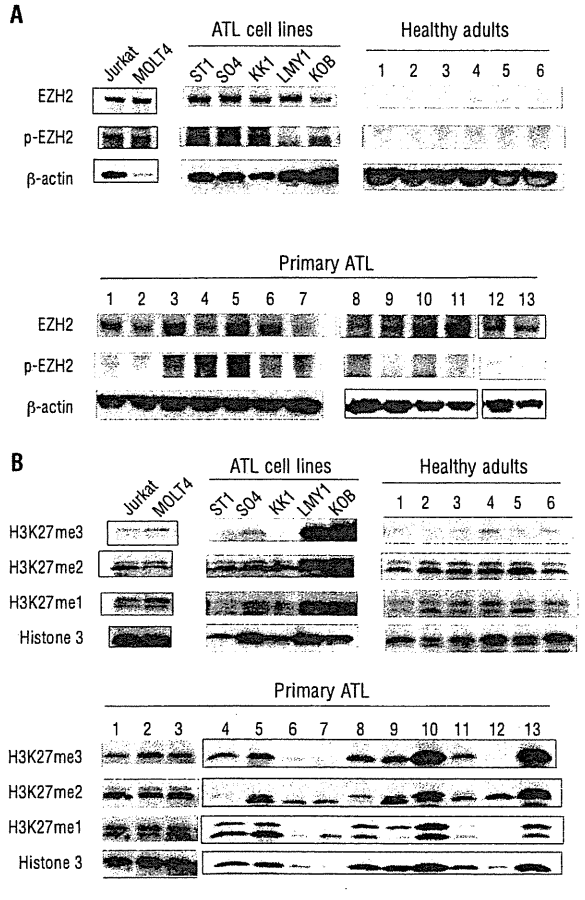

Figure 2. EZH2 protein expression and histone methylation. (A) Western blot analysis for EZH2 protein was performed on primary ATL cells, cells from healthy adults, and ATL cell lines. Primary ATL cells showed a clear 98-kDa band for EZH2 with the absence or presence of faint bands for phosphorylated EZH2 (p-EZH2). Cells from healthy adults hardly showed these bands. ATL cell lines ST1, SO4, and KK1 showed intense bands for both EZH2 and p-EZH2, but LM-Y1 and KOB cells showed intense bands for EZH2 with the absence of a band for p-EZH2. (B) Western blot analysis for histone methylation status was performed. Only primary ATL cells and LM-Y1 and KOB cell lines showed a clear band for H3K27me3, but others hardly showed the band. Bands for H3K27me2, H3K27me1, and histone H3 were observed in almost all samples examined.

Downregulation of miR-101 and miR-128a may be responsible for increased EZH2 expression

So far, more than 700 miRNAs have been identified in humans, and each miRNA regulates multiple target genes. miR-101 and miR-26a have been shown to be negative regulators of *EZH2* expression and are depressed in several types of cancer cells.[34,35] miR-128a is known to be a negative regulator of *BMI1* and has been reported to be involved in glioma cell proliferation.[36] We quantified these miRNAs in primary ATL cells and cells from HTLV-1 carriers to investigate the mechanism of *EZH2* overexpression. ATL cells showed significantly decreased levels of miR-101 and miR-128a compared with the cells from HTLV-1 carriers (Figure 3A and C). Notably, there were significant inverse correlations between *EZH2* expression and miR-101 expression or *EZH2* expression and miR-128a expression (Figure 3D and E), suggesting that decrease of these miRNAs accounts for the overexpression of *EZH2*. Since genomic loss of miR-101 has been reported in prostate cancer,[34] we performed quantitative genomic PCR for miR-101 in two loci, miR-101-1 (chromosome 1p31) and miR-101-2 (chromosome 9p24). Both loci were preserved in all 10 ATL samples examined (*Online Supplementary Figure S4*). The expression of miR-26a did not, in contrast, differ between ATL cells and cells from HTLV-1 carriers (Figure 3B). Unexpectedly, there was no significant correlation between *BMI1* expression and miR-128a expression (Figure 3F).

Adult T-cell leukemia/lymphoma cells are sensitive to DZNep and PS (LBH589)

We first examined the sensitivity of ATL-related cell lines and acute T-lymphoblastic leukemia cell lines to DZNep, an inhibitor of S-adenosylhomocysteine hydrolase, which has recently been shown to decrease the expression of EZH2 and histone methylation.[22,23] DZNep inhibited the proliferation of these cell lines, at concentrations above 0.5 μM (*Online Supplementary Figure S5A*). In contrast, $CD4^+$ T cells from healthy adults as a normal control were resistant to DZNep even at 5 μM. Notably, although DZNep decreased *EZH2* expression in ST1, SO4, and KK1, it did not decrease but rather increased the expression in KOB, results which were confirmed by Western blot (*Online Supplementary Figure S5B and C*). PS (LBH589) is also known to decrease the level of EZH2 in several types of leukemia cells.[24] One hundred nM of PS (LBH589) decreased *EZH2* expression at both transcript and protein levels in ATL cell lines including KOB and LM-Y1, which showed a similar EZH2 expression profile to that of primary ATL cells, namely, high EZH2 expression with low phosphorylated EZH2 and strong H3K27me3 (*Online Supplementary Figure S5D and E*). We next examined whether these agents show a synergistic effect or just an additive effect. As shown in *Online Supplementary Figure S5F* (upper panel), the cell viabilities of LM-Y1 treated with 25 nM PS (LBH589) or 2.5 μM DZNep were 70% and 87%, respectively. A combination of this setting (LBH:DZNep=1:100) markedly decreased the proportion of viable cells (40%) compared with that of cells treated

with either agent alone. Similarly, cell viabilities of KOB treated with 25 nM PS (LBH589), 2.5 μM DZNep, or a combination of these agents were 86%, 93%, and 48%, respectively. By calculating CI according to the method of Chou and Talalay,[29] we found a strong synergistic antiproliferative effect in both cell lines (*Online Supplementary Figure S5F*, lower panel).

Discussion

EZH2 is a critical component of PRC2, which mediates epigenetic gene silencing through trimethylation of H3K27.[37,38] EED and SUZ12 are also required for the exhibition of methyltransferase activity and for the localization of this complex to target genes.[39] In an analysis of genome-wide H3K27 methylation in aggressive prostate cancer tissues, a significant subset of the target genes were also targets in embryonic stem cells, suggesting that the mechanism for gene silencing used to maintain stem cell renewal is converted into oncogenesis.[40] Ectopic expression of EZH2 is capable of providing a proliferative advantage to primary cells, and its gene locus is amplified in primary tumors.[41] Indeed, increased EZH2 expression has been reported in several types of cancer cells, and its clinical significance is extensively studied in prostate cancer.[42] Amounts of both *EZH2* transcript and EZH2 protein were elevated in metastatic prostate cancer; in addition, clinically localized prostate cancers that express higher concentrations of *EZH2* showed a poorer prognosis. An association of increased EZH2 expression with poor prognosis has also been reported in other solid tumors. Currently, however, there are only limited reports describing EZH2 expression in hematologic malignancies.

In the present study, we showed for the first time that EZH2 was over-expressed in ATL cells, and that the increased EZH2 was not phosphorylated and was in its active form. The increased EZH2 seemed to exhibit histone methyltransferase activity *in vivo*, as supported by the results that ATL cells from both peripheral blood and lymph nodes were strongly positive for H3K27me3. Since EZH2 was almost undetectable in cells from healthy adults and HTLV-1 carriers, it is likely that deregulation of PRC2 caused by over-expressed EZH2 is involved in the early steps of ATL oncogenesis. Meanwhile, ATL patients with high EZH2 expression showed shorter survival than patients with low EZH2 expression, indicating that increased EZH2 also plays a role in the process of ATL progression. It has been reported that genes methylated in cancer cells are specifically packaged with nucleosomes containing H3K27.[43] However, there are only a few studies that actually examined H3K27me3 in primary tumor cells or tissues. In one such study, H3K27me3 expression was unexpectedly lower in breast, ovarian, and pancreatic cancers than in corresponding normal tissues, although it has been reported that there are increased levels of H3K27me3 in breast cancer cell lines.[44,45] We do not have an adequate explanation for these conflicts at present, but there may be some differences in the process of oncogenesis between solid tumors and hematologic malignancies.

The mechanism of the overexpression of EZH2 in tumors remains largely unknown. miRNAs regulate gene expression and play important roles in cellular differentiation and embryonic stem cell development. Recently, two miRNAs, miR-101 and miR-26a, were found to repress *EZH2* expression. The expression of miR-101 decreases in parallel with an increase in *EZH2* expression during progression in prostate tumors.[34] In addition to these miRNAs, we examined miR-128a, which has been shown to repress *BMI1* expression in glioblastoma, because overexpression of *BMI-1* is associated with the development of malignant lymphoma.[31,36] ATL cells showed a decreased level of miR-

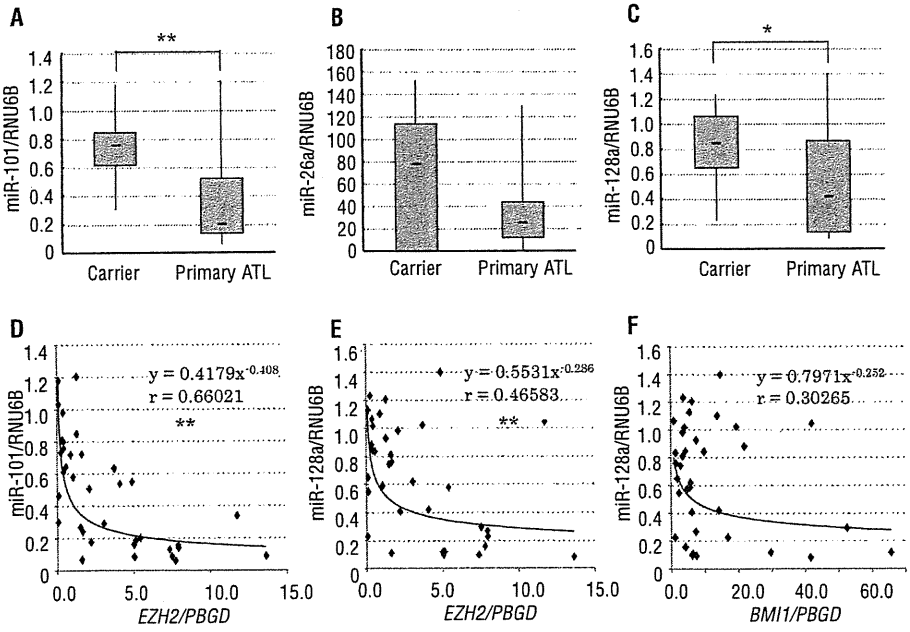

Figure 3. Quantitative real-time RT-PCR for miRNAs. (A-C) Expressions of miR-101 (A), miR-26a (B), and miR-128a (C) were compared between ATL patients and HTLV-1 carriers. Primary ATL cells showed significantly lower levels of miR-101 and miR-128a (Mann-Whitney's U test) compared with the cells from HTLV-1 carriers (A, C). There was no significant difference in miR-26a expression between the two groups (B). (D, E, F) Correlation between miRNA and *EZH2* or *BMI1* expression was examined. There were significant inverse correlations between normalized *EZH2* expression and miR-101 expression (D) or between normalized *EZH2* expression and miR-128a expression (E) (Spearman's correlation coefficient). In contrast, there was no correlation between normalized *BMI1* expression and miR-128a expression (F). $*P<0.05$, $**P<0.01$

101 expression compared with the cells from HTLV-1 carriers, which is not caused by genomic loss of the *miR-101* gene, in contrast to prostate cancer.[34] Moreover, there was a clear inverse correlation between *EZH2* expression and miR-101 expression, suggesting that increased *EZH2* is caused by the decrease in miR-101 expression. Although currently there is no report indicating an association of miR-128a with *EZH2* expression, miR-128a showed exactly the same pattern as miR-101, suggesting that the decrease in miR-128a also participates in *EZH2* overexpression in ATL. By analyzing the 3'-UTR sequence of *EZH2*, it has recently been shown that there are two predicted miR-101 target sites and one predicted miR-26a target site in the 3'-UTR of EZH2.[46] We performed a similar analysis and found that there was also a potential target site for miR-128a near one of the miR-101 target sites (*Online Supplementary Figure S6*). miR-26a was not decreased in ATL cells, and there was no correlation between miR-26a expression and *EZH2* expression or miR-128a expression and *BMI1* expression. The association of miR-26a with *EZH2* was found in normal cell differentiation as a physiological phenomenon but not in tumor cells. The miRNAs used to regulate normal development and differentiation may be different from those used for the development of tumors. Another possible explanation for the mechanism of increased *EZH2* expression in ATL is inactivation of *p14ARF/p15INK4B/p16INK4A* tumor suppressor genes, which frequently occurs in ATL.[14,15,19,20] EZH2 is a mólecule downstream of the pRB-E2F pathway, and inactivation of these genes allows E2F to be released from pRB, which results in the upregulation of *EZH2* expression.[41] Several recent reports indicate that EZH2 functions to repress the expression of *p14ARF/p15INK4B/p16INK4A*; therefore, increased EZH2 may be used to further decrease the expression of *p14ARF/p15INK4B/p16INK4A*.[47] Since somatic mutations altering EZH2 (Tyr641) have recently been reported in follicular and diffuse large B-cell lymphomas of germinal-center origin,[48] we performed a similar analysis in 10 primary ATL samples. There were however no such mutations (*Online Supplementary Figure S7*).

ATL is quite resistant to antineoplastic agents and the median survival time of those with the aggressive subtypes is only 13 months, even in a recent multicenter clinical trial.[49] Since high EZH2 expression with H3K27me3 seems to be an essential component for the initiation and promotion of cell proliferation in ATL, we searched for the possibility of therapeutic strategies targeting EZH2. We examined the sensitivity of ATL cells to agents that have been shown to inhibit *EZH2* expression and histone methylation. DZNep is a carbocyclic analog of adenosine synthesized more than 20 years ago as an inhibitor of S-adenosylhomocysteine hydrolase, which has therapeutic potential as an anticancer or antiviral drug.[21] DZNep has recently aroused interest for its unique features; it decreases the expressions of *EZH2*, *SUZ12*, and *EED* with inhibition of H3K27 methylation and induces apoptosis in cancer cells but not in normal cells.[22,23] ATL cell lines were sensitive to DZNep and their cell proliferation was attenuated at one-tenth of the concentration used in these studies. More interestingly, DZNep showed no toxicity to normal CD4+ T cells as a normal control. Acute T-lymphoblastic leukemia cell lines showed similar sensitivities to DZNep, which may indicate that DZNep exerts general toxicity to leukemia and lymphoma cells not necessarily associated with histone modification. Indeed, although DZNep rather increased EZH2 expression in KOB cells, this cell line was equally sensitive as other cell lines to DZNep. HDAC inhibitor PS (LBH589) is an effective agent for cutaneous T-cell lymphoma and induced complete remission in 2 of 9 patients involved in a phase I clinical trial.[50] More interestingly, it has been reported recently that combined use of DZNep and PS (LBH589) yielded more depletion of EZH2 and induced more apoptosis of leukemia cells, but not normal CD34 (+) bone marrow progenitor cells.[51] In the present study, we showed that the combination of DZNep and PS (LBH589) exhibited a synergistic effect in killing ATL cells. Thus, epigenetic therapy by the combined use of these agents that inhibit histone methylation could lead to a breakthrough in the treatment of aggressive ATL.

Authorship and Disclosures

The information provided by the authors about contributions from persons listed as authors and in acknowledgments is available with the full text of this paper at www.haematologica.org.

Financial and other disclosures provided by the authors using the ICMJE (www.icmje.org) Uniform Format for Disclosure of Competing Interests are also available at www.haematologica.org.

References

1. Sparmann A, van Lohuizen M. Polycomb silencers control cell fate, development and cancer. Nat Rev Cancer. 2006;6(11):846-56.
2. Lee TI, Jenner RG, Boyer LA, Guenther MG, Levine SS, Kumar RM, et al. Control of developmental regulators by Polycomb in human embryonic stem cells. Cell. 2006;125(2):301-13.
3. Kamminga LM, Bystrykh LV, de Boer A, Houwer S, Douma J, Weersing E, et al. The Polycomb group gene Ezh2 prevents hematopoietic stem cell exhaustion. Blood. 2006;107(5):2170-9.
4. van Lohuizen M, Tijms M, Voncken JW, Schumacher A, Magnuson T, Wientjens E. Interaction of mouse polycomb-group (Pc-G) proteins Enx1 and Enx2 with Eed: Indication for separate Pc-G complexes. Mol Cell Biol. 1998;18(6):3572-9.
5. Satijn DP, Hamer KM, den Blaauwen J, Otte AP. The Polycomb group protein EED interacts with YY1, and both proteins induce neural tissue in Xenopus embryos. Mol Cell Biol. 2001;21(4):1360-9.
6. van der Vlag J, Otte AP. Transcriptional repression mediated by the human polycomb-group protein EED involves histone deacetylation. Nat Genet. 1999;23(4):474-8.
7. Vire E, Brenner C, Deplus R, Blanchon L, Fraga M, Didelot C, et al. The Polycomb group protein EZH2 directly controls DNA methylation. Nature. 2006;439(7078):871-4.
8. Cao R, Zhang Y. The functions of E(Z)EZH2-mediated methylation of lysine 27 in histoneH3. Curr Opin Genet Dev. 2004;14(2):155-64.
9. Widschwendter M, Fiegl H, Egle D, Mueller-Holzner E, Spizzo G, Marth C, et al. Epigenetic stem cell signature in cancer. Nat Genet. 2007;39(2):157-8.
10. Simon JA, Lange CA. Roles of the EZH2 histone methyltransferase in cancer epigenetics. Mutat Res. 2008;647(1-2):21-9.
11. Uchiyama T, Yodoi J, Sagawa K, Takatsuki K, Uchino H. Adult T-cell leukemia: clinical and hematologic features of 16 cases. Blood. 1977;50(3):481-92.
12. Yoshida M, Seiki M, Yamaguchi K, Takatsuki K. Monoclonal integration of human T-cell leukemia provirus in all primary tumors of adult T-cell leukemia suggests causative role of human T-cell leukemia virus in the disease. Proc Natl Acad Sci USA. 1984;81(8):2534-7.
13. Shimoyama M and members of the Lymphoma Study Group (1984-1987):

Diagnostic criteria and classification of clinical subtypes of adult T-cell leukaemia-lymphoma. A report from the Lymphoma Study Group (1984-1987). Br J Haematol. 1991;79(3):428-37.
14. Hatta Y, Hirama T, Miller CW, Yamada Y, Tomonaga M, Koeffler HP. Homozygous deletions of p15 (MTS2) and p16 (CDKN2/MTS1) genes in adult T-cell leukemia. Blood. 1995;85(10):2699-704.
15. Yamada Y, Hatta Y, Murata K, Sugawara K, Ikeda S, Mine M, et al. Deletions of p15 and/or p16 genes as a poor-prognosis factor in adult T-cell leukemia. J Clin Oncol. 1997;15(5):1778-85.
16. Nagai H, Kinoshita T, Imamura J, Murakami Y, Hayashi K, Mukai K, et al. Genetic alteration of p53 in some patients with adult T-cell leukemia. Jpn J Cancer Res. 1991;82(12):1421-7.
17. Sakashita A, Hattori T, Miller CW, Suzushima H, Asou N, Takatsuki K, et al. Mutations of the p53 gene in adult T-cell leukemia. Blood. 1992;79(2):477-80.
18. Tawara M, Hogerzeil SJ, Yamada Y, Takasaki Y, Soda H, Hasegawa H, et al. Impact of p53 aberration on the progression of adult T-cell leukemia/lymphoma. Cancer Lett. 2006;234(2):249-55.
19. Kohno T, Yamada Y, Tawara M, Takasaki Y, Kamihira S, Tomonaga M, et al. Inactivation of p14ARF as a key event for the progression of adult T-cell leukemia/lymphoma. Leuk Res. 2007;31(12):1625-32.
20. Nosaka K, Maeda M, Tamiya S, Sakai T, Mitsuya H, Matsuoka M. Increasing methylation of the CDKN2A gene is associated with the progression of adult T-cell leukemia. Cancer Res. 2000;60(4):1043-8.
21. Glazer RI, Hartman KD, Knode MC, Richard MM, Chiang PK, Tseng CK, et al. 3-Deazaneplanocin: a new and potent inhibitor of S-adenosylhomocysteine hydrolase and its effects on human promyelocytic leukemia cell line HL-60. Biochem Biophys Res Commun. 1986;135 (2):688-94.
22. Miranda TB, Cortez CC, Yoo CB, Liang G, Abe M, Kelly TK, et al. DZNep is a global histone methylation inhibitor that reactivates developmental genes not silenced by DNA methylation. Mol Cancer Ther. 2009;8(6):1579-88.
23. Tan J, Yang X, Zhuang L, Jiang X, Chen W, Lee PL, et al. Pharmacologic disruption of Polycomb-repressive complex 2-mediated gene repression selectively induces apoptosis in cancer cells. Genes Dev. 2007;21(9): 1050-63.
24. Fiskus W, Pranpat M, Balasis M, Herger B, Rao R, Chinniyan A, et al. Histone deacetylase inhibitors deplete EZH2 and associated Polycomb Repressive Complex 2 proteins with attenuation of HOXA9 and MEIS1 and loss of survival of human acute leukemia cells. Mol Cancer Ther. 2006;5 (12):3096-104.
25. Choi YL, Tsukasaki K, O'Neill MC, Yamada Y, Onimaru Y, Matsumoto K, et al. A genomic analysis of adult T-cell leukemia. Oncogene. 2007;26(8):1245-55.
26. Yamada Y, Ohmoto Y, Hata T, Yamamura M, Murata K, Tsukasaki K, et al. Features of the cytokines secreted by adult T cell leukemia (ATL) cells. Leuk Lymphoma. 1996;21(5-6):443-7.
27. Choi YL, Makishima H, Ohashi J, Yamashita Y, Ohki R, Koinuma K, et al. DNA microarray analysis of natural killer cell-type lymphoproliferative disease of granular lymphocytes with purified CD3(-) CD56(+) fractions. Leukemia. 2004;18(3): 556-65.
28. Hasegawa H, Yamada Y, Komiyama K, Hayashi M, Ishibashi M, Sunazuka T, et al. A novel natural compound, a cycloanthranilylproline derivative (Fuligocandin B), sensitizes leukemia cells to apoptosis induced by tumor necrosis factor related apoptosis-inducing ligand (TRAIL) through 15-deoxy-Delta 12, 14 prostaglandin J2 production. Blood. 2007;110(5):1664-74.
29. Chou TC, Talalay P. Quantitative analysis of dose-effect relationships: the combined effects of multiple drugs or enzyme inhibitors. Adv Enzyme Regul. 1984;22:27-55.
30. Yasunaga J, Taniguchi Y, Nosaka K, Yoshida M, Satou Y, Sakai T, et al. Identification of aberrantly methylated genes in association with adult T-cell leukemia. Cancer Res. 2004;64(17):6002-9.
31. Jacobs JJ, Kieboom K, Marino S, DePinho RA, van Lohuizen M. The oncogene and Polycomb-group gene bmi-1 regulates cell proliferation and senescence through the ink4a locus. Nature. 1999;397(6715):164-8.
32. Scott CL, Gil J, Hernando E, Teruya-Feldstein J, Narita M, Martinez D, et al. Role of the chromobox protein CBX7 in lymphomagenesis. Proc Natl Acad Sci USA. 2007;104(13):5389-94.
33. Cha TL, Zhou BP, Xia W, Wu Y, Yang CC, Chen CT, et al. Akt-mediated phosphorylation of EZH2 suppresses methylation of Lysine 27 in histone H3. Science. 2005;310(5746):306-10.
34. Varambally S, Cao Q, Mani RS, Shankar S, Wang X, Ateeq B, et al. Genomic loss of microRNA-101 leads to overexpression of histone methyltransferase EZH2 in cancer. Science. 2008;322(5908):1695-6.
35. Sander S, Bullinger L, Klapproth K, Fiedler K, Kestler HA, Barth TF, et al. MYC stimulates EZH2 expression by repression of its negative regulator miR-26a. Blood. 2008; 112(10):4202-12.
36. Godlewski J, Nowicki MO, Bronisz A, Williams S, Otsuki A, Nuovo G, et al. Targeting of the Bmi-1 oncogene/stem cell renewal factor by microRNA-128 inhibits glioma proliferation and self-renewal. Cancer Res. 2008;68(22):9125-30.
37. Cao R, Wang L, Wang H, Xia L, Erdjument-Bromage H, Tempst P, et al. Role of histone H3 lysine 27 methylation in Polycomb-group silencing. Science. 2002;298(5595): 1039-43.
38. Czermin B, Melfi R, McCabe D, Seitz V, Imhof A, Pirrotta V. Drosophila enhancer of Zeste/ESC complexes have a histone H3 methyltransferase activity that marks chromosomal Polycomb sites. Cell. 2002;111(2): 185-96.
39. Cao R, Zhang YI. SUZ12 is required for both the histone methyltransferase activity and the silencing function of the EED-EZH2 complex. Mol Cell. 2004;15(1):57-67.
40. Yu J, Yu J, Rhodes DR, Tomlins SA, Cao X, Chen G, et al. A polycomb repression signature in metastatic prostate cancer predicts cancer outcome. Cancer Res. 2007; 67(22):10657-63.
41. Bracken AP, Pasini D, Capra M, Prosperini E, Colli E, Helin K. EZH2 is down stream of the pRB-E2F pathway, essential for proliferation and amplified in cancer. EMBO J. 2003;22(20):5323-35.
42. Varambally S, Dhanasekaran SM, Zhou M, Barrette TR, Kumar-Sinha C, Sanda MG, et al. The polycomb group protein EZH2 is involved in progression of prostate cancer. Nature. 2002;419(6907):624-9.
43. Schlesinger Y, Straussman R, Keshet I, Farkash S, Hecht M, Zimmerman J, et al. Polycomb-mediated methylation of Lys27 of histone H3 pre-marks genes for de novo methylation in cancer. Nat Genet. 2007;39 (2):232-6.
44. Wei Y, Xia W, Zhang Z, Liu J, Wang H, Adsay NV, et al. Loss of trimethylation at lysine 27 of histone H3 is a predictor of poor outcome in breast, ovarian, and pancreatic cancers. Mol Carcinog. 2008;47 (9):701-6.
45. Sun F, Chan E, Wu Z, Yang X, Marquez VE, Yu Q. Combinatorial pharmacologic approaches target EZH2-mediated gene repression in breast cancer cells. Mol Cancer Ther. 2009;8(12):3191-202.
46. Cao P, Deng Z, Wan M, Huang W, Cramer SD, Xu J, et al. MicroRNA-101 negatively regulates Ezh2 and its expression is modulated by androgen receptor and HIF-1alpha/HIF-1beta. Mol Cancer. 2010;9: 108.
47. Bracken AP, Kleine-Kohlbrecher D, Dietrich N, Pasini D, Gargiulo G, Beekman C, et al. The polycomb group proteins bind throughout the INK4A-ARF locus and are disassociated in senescent cells. Genes Dev. 2007;21(5):525-30.
48. Morin RD, Johnson NA, Severson TM, Mungall AJ, An J, Goya R, et al. Somatic mutations altering EZH2 (Tyr641) in follicular and diffuse large B-cell lymphomas of germinal-center origin. Nat Genet. 2010; 42(2):181-5.
49. Yamada Y, Tomonaga M, Fukuda H, Hanada S, Utsunomiya A, Tara M, et al. A new G-CSF-supported combination chemotherapy, LSG15, for adult T-cell leukaemia-lymphoma: Japan Clinical Oncology Group Study 9303. Br J Haematol. 2001;113(2):375-82.
50. Ellis L, Pan Y, Smyth GK, George DJ, McCormack C, Williams-Truax R, et al. Histone deacetylase inhibitor panobinostat induces clinical responses with associated alterations in gene expression profiles in cutaneous T-cell lymphoma. Clin Cancer Res. 2008;14(14):4500-10.
51. Fiskus W, Wang Y, Sreekumar A, Buckley KM, Shi H, Jillella A, et al. Combined epigenetic therapy with the histone methyltransferase EZH2 inhibitor 3-deazaneplanocin A and the histone deacetylase inhibitor panobinostat against human AML cells. Blood. 2009;114(13):2733-43.

From bloodjournal.hematologylibrary.org at Jichi Medical School Library on February 16, 2012. For personal use only.

blood

2011 118: 6881-6892
Prepublished online October 31, 2011;
doi:10.1182/blood-2011-05-354654

miR-135b mediates NPM-ALK–driven oncogenicity and renders IL-17–producing immunophenotype to anaplastic large cell lymphoma

Hironori Matsuyama, Hiroshi I. Suzuki, Hikaru Nishimori, Masaaki Noguchi, Takashi Yao, Norio Komatsu, Hiroyuki Mano, Koichi Sugimoto and Kohei Miyazono

Updated information and services can be found at:
http://bloodjournal.hematologylibrary.org/content/118/26/6881.full.html

Articles on similar topics can be found in the following Blood collections
Lymphoid Neoplasia (1027 articles)

Information about reproducing this article in parts or in its entirety may be found online at:
http://bloodjournal.hematologylibrary.org/site/misc/rights.xhtml#repub_requests

Information about ordering reprints may be found online at:
http://bloodjournal.hematologylibrary.org/site/misc/rights.xhtml#reprints

Information about subscriptions and ASH membership may be found online at:
http://bloodjournal.hematologylibrary.org/site/subscriptions/index.xhtml

Blood (print ISSN 0006-4971, online ISSN 1528-0020), is published weekly by the American Society of Hematology, 2021 L St, NW, Suite 900, Washington DC 20036.
Copyright 2011 by The American Society of Hematology; all rights reserved.

From bloodjournal.hematologylibrary.org at Jichi Medical School Library on February 16, 2012. For personal use only.

miR-135b mediates NPM-ALK–driven oncogenicity and renders IL-17–producing immunophenotype to anaplastic large cell lymphoma

*Hironori Matsuyama,[1] *Hiroshi I. Suzuki,[1] Hikaru Nishimori,[1] Masaaki Noguchi,[2] Takashi Yao,[3] Norio Komatsu,[4] Hiroyuki Mano,[5,6] Koichi Sugimoto,[4] and Kohei Miyazono[1]

[1]Department of Molecular Pathology, Graduate School of Medicine, University of Tokyo, Tokyo, Japan; [2]Department of Hematology, Juntendo Urayasu Hospital, Chiba, Japan; [3]Department of Human Pathology and [4]Division of Hematology, Department of Internal Medicine, Juntendo University School of Medicine, Tokyo, Japan; [5]Department of Medical Genomics, Graduate School of Medicine, University of Tokyo, Tokyo, Japan; and [6]Division of Functional Genomics, Jichi Medical University, Tochigi, Japan

Many transformed lymphoma cells show immune-phenotypes resembling the corresponding normal lymphocytes; thus, they provide a guide for proper diagnosis and present promising routes to improve their pathophysiologic understanding and to identify novel therapeutic targets. However, the underlying molecular mechanism(s) of these aberrant immune-phenotypes is largely unknown. Here, we report that microRNA-135b (miR-135b) mediates nucleophosmin-anaplastic lymphoma kinase (NPM-ALK)–driven oncogenicity and empowers IL-17–producing immunophenotype in anaplastic large cell lymphoma (ALCL). NPM-ALK oncogene strongly promoted the expression of miR-135b and its host gene LEMD1 through activation of signal transducer and activator of transcription (STAT) 3. In turn, elevated miR-135b targeted FOXO1 in ALCL cells. miR-135b introduction also decreased chemosensitivity in Jurkat cells, suggesting its contribution to oncogenic activities of NPM-ALK. Interestingly, miR-135b suppressed T-helper (Th) 2 master regulators STAT6 and GATA3, and miR-135b blockade attenuated IL-17 production and paracrine inflammatory response by ALCL cells, indicating that miR-135b–mediated Th2 suppression may lead to the skewing to ALCL immunophenotype overlapping with Th17 cells. Furthermore, antisense-based miR-135b inhibition reduced tumor angiogenesis and growth in vivo, demonstrating significance of this "Th17 mimic" pathway as a therapeutic target. These results collectively illuminated unique contribution of oncogenic kinase-linked microRNA to tumorigenesis through modulation of tumor immune-phenotype and microenvironment. (*Blood.* 2011;118(26):6881-6892)

Introduction

MicroRNAs (miRNAs) are endogenous noncoding, 20- to 23-nucleotide single-stranded RNAs that negatively regulate gene expression in a sequence-specific manner.[1] miRNA species are generated through RNase-mediated processing reaction by two central RNases III, Drosha and Dicer, from long primary transcripts (primary miRNAs [pri-miRNAs]) and incorporated along with core Argonaute proteins into the RNA-induced silencing complex. RNA-induced silencing complex interacts mainly with 3′ untranslated region (UTR) of target mRNAs through partial base complementarity to the 5′ miRNA seed region, leading to degradation, destabilization, or translational inhibition of target mRNAs. miRNAs regulate differentiation and functions of various cell types, including immune cells in a highly context-dependent manner.[2]

Alteration of miRNome has emerged as a key feature of cancer-associated dysfunction of gene regulatory networks. Although miRNA dysregulation affects cancer cell behavior with other genetic and epigenetic abnormalities, full pictures of their causes and consequences remain to be elucidated.[3] In hematologic malignancies, many transformed lymphoma cells show immune-phenotypes resembling the corresponding normal lymphocytes; thus, they represent a guide for proper diagnosis and promising routes to improve our understanding of their pathogenesis and to identify novel therapeutic targets.[4] For example, diffuse large B-cell lymphomas have been shown to be composed of at least 2 prognostic entities, depending on its resemblance to normal germinal center or activated B cells.[5] However, the molecular basis shaping the aberrant immunophenotypes of tumor cells has been largely unknown, and the relationship between miRNA regulation and lymphoma phenotype has not been investigated.

Recent studies revealed several mechanisms regulating miRNA expression.[6] Although certain oncoproteins, including Myc and tumor suppressors such as p53, have been linked to the regulation of miRNA expression,[7,8] involvement of oncogenic tyrosine kinases remains unclear in this regulatory pathway. Anaplastic lymphoma kinase (ALK) exerts characteristic oncogenic activities through fusion to several gene partners or mutations both in hematopoietic and nonhematopoietic solid tumors.[9,10] Nucleophosmin (NPM)–ALK is a representative translocation-dependent fusion-type oncogenic tyrosine kinase in anaplastic large cell lymphoma (ALCL). Although NPM-ALK drives malignant transformation of ALCL cells through various molecular mechanisms, including activation of signal transducer and activator of transcription (STAT) 3, Ras-ERK, and PI3K oncogenic signaling pathways,[9] involvement of miRNAs has not been reported so far. Here, we have explored unrecognized involvement of miRNAs in the downstream of NPM-ALK.

Submitted May 12, 2011; accepted October 25, 2011. Prepublished online as *Blood* First Edition paper, October 31, 2011; DOI 10.1182/blood-2011-05-354654.

*H.M. and H.I.S. contributed equally to this study.

The online version of the article contains a data supplement.

The publication costs of this article were defrayed in part by page charge payment. Therefore, and solely to indicate this fact, this article is hereby marked "advertisement" in accordance with 18 USC section 1734.

© 2011 by The American Society of Hematology

From bloodjournal.hematologylibrary.org at Jichi Medical School Library on February 16, 2012. For personal use only.

We identified miR-135b as one of the major downstream executors of NPM-ALK chimeric oncoprotein in ALCL. NPM-ALK strongly promoted the expression of miR-135b and its host gene LEMD1 through STAT3 activation. The elevated miR-135b targeted FOXO1 tumor suppressor. Interestingly, we further revealed the immune modulatory property of miR-135b shaping the T-cell phenotypes of ALCL cells. miR-135b suppressed T-helper (Th) 2 master regulators STAT6 and GATA3, and the blockade of miR-135b attenuated IL-17 production and paracrine inflammatory response by ALCL cells, suggesting that miR-135b–mediated Th2 suppression may skew the ALCL immunophenotype to overlap with that of Th17 cells. Antisense-based miR-135b inhibition reduced tumor angiogenesis and growth in vivo, underscoring the pathogenic roles of this pathway. Our findings revealed that miR-135b is involved in NPM-ALK–driven tumorigenesis and modulation of ALCL immunophenotype, and they also suggest dynamic commitment of miRNAs to mutual regulation between Th cell differentiation programs and determination of polarized immunophenotypes of malignant cells.

Methods

Cell lines and reagents

Karpas 299, SUDHL-1, and SUP-M2 cell lines were obtained from the German Collection of Microorganisms and Cell Cultures. Jurkat, Molt4, CCRF-CEM, HCT116, HEK293T, HeLa, and lung cancer cell lines were obtained from the American Type Culture Collection. WI-38 human diploid fibroblast line was obtained from the RIKEN Cell Bank. Human normal peripheral blood pan T lymphocytes were purchased from AllCells. Neuroblastoma cell lines were kindly provided from R. Sakai (National Cancer Center Research Institute, Tokyo, Japan). Hematologic, neuroblastoma, and lung cancer cell lines were maintained in RPMI-1640 (Invitrogen) containing 10% FBS, 100 units/mL penicillin, and 100 μg/mL streptomycin. Other cell lines were maintained in Dulbecco modified eagle medium (Invitrogen) with 10% FBS. In coculture experiment, Karpas 299 and WI-38 cells were cocultured (in Opti-MEM [Invitrogen] with 1% FBS) for 48 hours using Transwell tissue culture inserts (0.4-μm pore size; BD Biosciences). The following antibodies were used: ALK 4C5B8 (Invitrogen); STAT3 124H6, p-STAT3 D3A7, Akt 9272, p-Akt 193H12, FOXO1 C29H4, and STAT6 9362 (Cell Signaling Technology); p21 H-164, p27 F-8, and GATA3 HG3-31 (Santa Cruz Biotechnology); CREG1 299133 (R&D Systems); CD31 555024 (BD Biosciences); and α-tubulin DM-1A (Sigma-Aldrich). Kinase inhibitors (WHI-P154, U0126 and LY294002) were purchased from Calbiochem.

Patient samples

ALCL patients were diagnosed at Juntendo University Hospital and Juntendo Urayasu Hospital. Investigations were carried out in accordance with ethical standards authorized by the ethics committees of University of Tokyo, Juntendo University School of Medicine, and Jichi Medical University. Written informed consent was obtained in accordance with the Declaration of Helsinki.

TuD miRNA system, shRNA, and plasmids

Tough decoy RNA (TuD RNA) against miR-135b was designed according to a previous report.[11] Detailed structures of TuD RNA are described in supplemental Table 1 (available on the *Blood* Web site; see the Supplemental Materials link at the top of the online article). shRNAs were designed as described previously.[12,13] TuD RNAs and shRNAs were introduced into pENTR-H1 vector. Pri-miRNA expression vectors were generated by cloning short fragments of pri-miRNAs containing pre-miRNA and flanking sequence on both sides of pre-miRNA into pcDNA6.2-GW/EmGFP-miR (Invitrogen). miRNA sensor vectors were prepared by inserting mature miRNA complementary sequences within the XhoI and NotI sites of the 3′UTR of the luciferase gene in the Psicheck 2 dual luciferase reporter vector (Promega). For other reporter constructs, the 3′UTR segment of each target gene was cloned into the same luciferase reporter vector. The primer sequences used are given in supplemental Table 2. For transient transfection, pre-miR miRNA precursors (Ambion) also were used.

Luciferase reporter assay

Cells were transfected with each reporter construct with pri-miRNA expression vector using Lipofectamine 2000 (Invitrogen). Cell extracts were prepared 24 to 48 hours after transfection, and the ratio of *Renilla* to firefly luciferase was measured using the Dual-Luciferase Reporter Assay System (Promega).

qRT-PCR assays

Quantitative (q)RT-PCR assays were performed as described previously.[8] For detection of mRNAs, total RNA was extracted by TRIzol (Invitrogen) and subjected to reverse transcription using the PrimeScriptII first-strand cDNA synthesis kit (Takara) according to the manufacturer's instructions. qRT-PCR was performed with the 7500 Fast Real-Time PCR System (Applied Biosystems). The expression levels of mature miRNAs were determined using TaqMan MicroRNA assay kit (Applied Biosystems) according to the manufacturer's protocol. Data analysis was done by the comparative C_T method. Results were normalized to β-actin for pri-miRNA detection, and RNU44 small nucleolar RNA for evaluation of mature miRNA. miRNeasy mini kit (QIAGEN) or RecoverAll total nucleic acid isolation kit for FFPE Tissues (Ambion) was used for RNA extraction from clinical samples. The primer sequences used are given in supplemental Table 3.

Chromatin immunoprecipitation analysis

Cells were fixed by adding formaldehyde and then harvested. After sonication, samples were incubated at 4°C overnight with protein A or anti–mouse IgG-Dynabeads that had been preincubated with 5 to 10 μg of antibodies in PBS and 0.5% BSA. To precipitate STAT3, anti-STAT3 antibody 124H6 (Cell Signaling Technology) was used. Immunoprecipitated samples were eluted and reverse-crosslinked by incubation overnight at 65°C. Genomic DNA was then extracted with a PCR purification kit (QIAGEN) and subjected to PCR analysis. The primer sequences used are given in supplemental Table 3.

Lentiviral gene transfer

TuD RNAs, shRNAs, pri-miRNA, NPM-ALK, or mouse constitutively active (ca)–STAT3 (A662C/N664C)[14] was introduced by lentiviral infection system (a kind gift from H. Miyoshi, RIKEN, Tsukuba, Japan). TuD RNAs and shRNAs were transferred into lentivirus vector CS-RfA-EG via pENTR-H1 vector using LR clonase. Pri-miRNA was similarly transferred into CSII-EF-RfA-CMV-Puro lentivirus vector using pENTR vector. The lentivirus production was carried out by transfection of HEK293FT cells with the vector construct pCMV-VSV-G-RSV-Rev and pCAG-HIVgp. The viral particles were collected 48 hours after transfection, titered by Lenti-X qRT-PCR titration kit (Takara), introduced to cultured cells, and monitored by flow cytometric analysis to determine infection efficiency.

Immunoblot assay

Cells were lysed with a buffer containing 1% Nonidet P-40, 20mM Tris-HCl, pH 7.4, 150mM NaCl, 5mM EDTA, and 1% protease inhibitor mixture (Nacalai Tesque). Total cell lysates were subjected to SDS-PAGE and transferred to Fluoro Trans W membrane (Pall). Immunoblotting was performed using the indicated antibodies.

Drug sensitivity assay

Jurkat cells were seeded at a density of 1×10^5/mL and split 24 hours before treatment. After 24-hour treatment with different concentrations of cytosine β-D-arabinofuranoside (Sigma-Aldrich), cells were collected,

From bloodjournal.hematologylibrary.org at Jichi Medical School Library on February 16, 2012. For personal use only.

washed, and reseeded for assay of cell viability and apoptosis. Cell viability and apoptosis were assessed by WST-8 colorimetric assay (Nacalai Tesque) and annexin V assay kit (BD Biosciences), respectively.

ELISA

After transfection with miRCURY LNA microRNA power inhibitor (EXIQON; Control A or antisense against miR-135b), IL-17F concentrations in the culture supernatant (72 hours) of Karpas 299 cells were determined by ELISA kit (R&D Systems; Duoset human IL17F), according to the manufacturer's instructions.

In vivo cancer models

C.B-17/IcrCrj severe combined immunodeficient (SCID) female mice (4 weeks of age) were obtained from Charles River Japan. All animal experimental protocols were performed in accordance with the policies of the Animal Ethics Committee of the University of Tokyo. Karpas 299 cells (1×10^6; n = 6/group) were subcutaneously injected in 0.2 mL of a mixture of RPMI-1640 without FBS and 30% Matrigel (BD Biosciences) into female SCID mice and allowed to grow for 1 week to reach a volume of 50 to 200 mm^3. Complexes of miRCURY LNA microRNA power inhibitor (EXIQON; Control A or antisense against miR-135b) and atelocollagen (Koken) were prepared according to the manufacturer's instructions. Antisense oligonucleotides (5μM) with atelocollagen in a 200-μL volume were administered into the subcutaneous spaces around the tumors at days 7 and 10 after inoculation. Subcutaneous xenografts were measured externally every day until the end of evaluation periods, and tumor volume was approximated using the equation vol = $(a \times b^2)/2$, where vol is volume, a the length of the major axis, and b the length of the minor axis.

Immunohistochemistry

Tumor samples excised from the animals were fixed for 1 hour in 10% neutral-buffered formalin at room temperature, washed overnight in PBS containing 10% sucrose at 4°C, and embedded in optimal cutting temperature compound (Tissue-Tek). The samples were then snap-frozen in dry-iced acetone for immunohistochemistry. Frozen samples were further sectioned at 10-μm thickness in a cryostat, briefly fixed with 10% formalin, and then incubated with primary and secondary antibodies. Samples were observed using an LSM510 Meta confocal microscope (Carl Zeiss). Quantification of CD31-stained areas was performed in multiple fields on tumor sections from 6 mice using Photoshop 8.0.1 software (Adobe Systems) and ImageJ 1.36b software (National Institutes of Health).

GEP analysis

Microarray data for NPM-ALK gene expression signature (GSE6184) and clinical gene expression profiling (GEP) data of peripheral T-cell lymphoma (PTCL) patient samples (GSE19069) were obtained from the National Center for Biotechnology Information's Gene Expression Omnibus.[12,15] Gene-set enrichment analysis (GSEA) was performed with GSEA Version 2.0 software available from the Broad Institute (http://www.broadinstitute.org/gsea/) using microarray data for NPM-ALK signature (GSE6184) and GSEA-embedded potential miRNA target gene sets or TargetScan-predicted putative miRNA target lists (http://www.targetscan.org/).[16]

Statistical analysis

Statistical analysis was performed using the Student t test or multivariate ANOVA (for proliferation assay and in vivo analysis; $*P < .05$; $**P < .01$; $***P < .001$). All data are expressed as mean ± SEM.

Results

Up-regulation of miR-135b in ALCL

Previous microarray analysis on miRNA expression identified various signatures of aberrant miRNA expression in a wide range of hematologic cell lines, including major types of B- and T-cell lymphoma, lymphoproliferative disorder, T-cell acute lymphoblastic leukemia, and acute myeloid leukemia.[17] In this analysis, ALCL was characterized by increased expression of miR-135b, miR-21, and miR-27a.[17] We verified the observation using quantitative RT-PCR analysis on 3 ALCL cell lines carrying *NPM-ALK* fusion; Karpas 299, SUDHL-1, and SUP-M2 (Figure 1A-C). Among these miRNAs, miR-135b was most prominently up-regulated in ALCL cell lines, and it was reduced by the ALK inhibitor WHI-P154 (Figure 1D), prompting us to track potential downstream effector(s) of NPM-ALK to miR-135b. Because miR-135b is located in the first intron of the LEM domain containing 1 (*LEMD1*) gene on 1q32.1 (Figure 1E), we examined LEMD1 expression levels in ALCL cell lines. LEMD1 was also remarkably elevated in ALCL cells (Figure 1F). ALK inhibition resulted in a potent decrease of LEMD1 and primary transcript of miR-135b (pri-miR-135b) in Karpas 299 and SUDHL-1 cells (Figure 1G), as well as in mature miR-135b, suggesting that NPM-ALK characterizes high miR-135b expression in ALCL cells. The effects of WHI-P154 on mature miR-135b were lower than those on pri-miR-135b, possibly because of generally high stability of mature miRNAs. In addition, we measured miR135b expression levels in clinical samples of ALCL patients and found that miR-135b is elevated in human primary ALK-positive ALCL samples, compared with reactive lymph node and ALK-negative ALCL samples (Figure 1H).

NPM-ALK induces LEMD1/miR-135b through STAT3 activation

To examine a direct involvement of NPM-ALK in miR-135b up-regulation in ALCL cells, we introduced wild-type and kinase-dead NPM-ALK into the human Jurkat cells and examined the expression levels of LEMD1 and miR-135b. NPM-ALK but not kinase-dead NPM-ALK (K210R) induced both LEMD1 and mature miR-135b in Jurkat cells (Figure 2A), indicating that NPM-ALK up-regulates the host gene and subsequently miR-135b through the kinase activity.

Because previous reports demonstrated that NPM-ALK elicits many downstream pathways, including STAT3, Ras-ERK, and PI3K signaling pathways,[9] we next examined the involvement of these pathways. Knockdown of NPM-ALK or STAT3 suppressed the expression of LEMD1 and miR-135b in ALCL cells (Figure 2B and supplemental Figure 1A),[12,13] whereas inhibition of ERK or PI3K failed to exert such effects (supplemental Figure 1B). We also confirmed that ca-STAT3 up-regulates LEMD1 and miR-135b in Jurkat cells (Figure 2C). Furthermore, we analyzed putative STAT3-binding sites within the conserved region of *LEMD1* gene between human and mouse and showed that STAT3 binds to putative STAT3-binding sites within the *LEMD1* genomic region by chromatin-immunoprecipitation analysis (Figure 2D-E). Reflecting high miR-135b expression, luciferase expression levels from miR-135b sensor vector were remarkably lower than those from control sensor vector in ALCL cells but not in Jurkat cells, confirming that miR-135b is highly active in ALCL cells (Figure 2F). Taken together, these results demonstrate that miR-135b lies downstream of the NPM-ALK/STAT3 signaling pathway in ALCL.

miR-135b targets FOXO1 and regulates chemosensitivity

Several potential targets of miR-135b with tumor-suppressive activities were computationally predicted previously[18] and included APC, LZTS1, LATS2, CREG1, and FOXO1. APC has been already shown as a target of miR-135b,[19] and we validated LZTS1, LATS2, and FOXO1 using luciferase reporter assay (supplemental

From bloodjournal.hematologylibrary.org at Jichi Medical School Library on February 16, 2012. For personal use only.

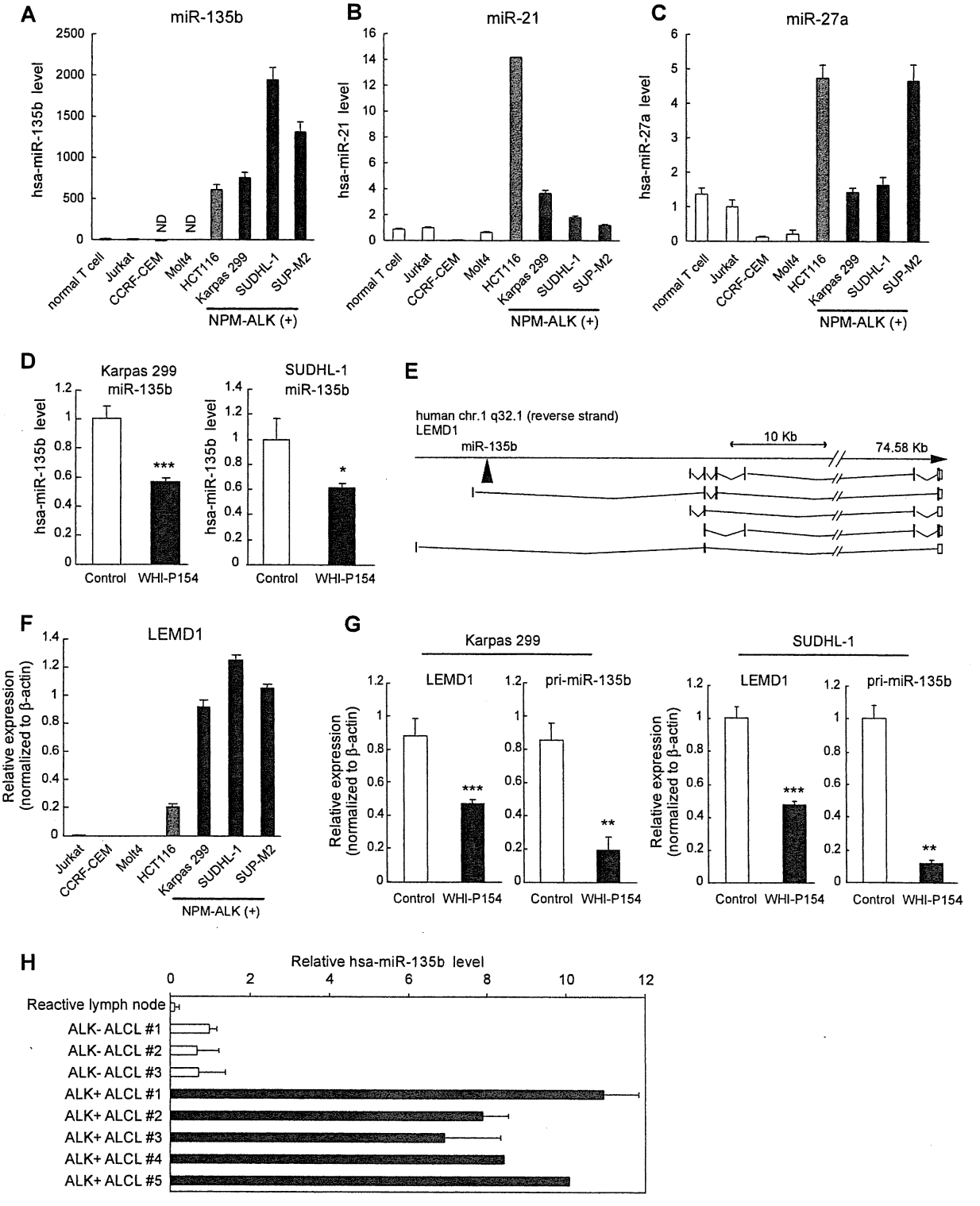

Figure 1. High expression of miR-135b and LEMD1 in ALCL. (A-C) Expression of mature miR-135b (A), miR-21 (B), and miR-27a (C) in NPM-ALK (+) ALCL cell lines (Karpas 299, SUDHL-1, and SUP-M2), normal T lymphocytes, and several T-lymphoblastic leukemia cell lines (Jurkat, CCRF-CEM, and Molt4), detected by qRT-PCR analysis. HCT116 colon cancer cells expressing endogenous miR-135b were used as positive control. ND indicates not detected. (D) Attenuation of miR-135b expression by ALK inhibitor WHI-P154. Mature miR-135b in Karpas 299 and SUDHL-1 cells was analyzed by qRT-PCR after WHI-P154 treatment (10μM, 4 hours). (E) Schematic diagram of genomic organization of human *LEMD1* gene and miR-135b. As for human *LEMD1*, several splicing variants have been reported. miR-135b is located in the first intron of *LEMD1* longer transcripts. (F) High expression of LEMD1 in ALCL cells, determined as in panel A. (G) Suppression of LEMD1 and pri-miR-135b by WHI-P154 (10μM, 1 hour) in Karpas 299 and SUDHL-1 cells, assessed as in panel D (*$P < .05$; **$P < .01$; ***$P < .001$). (H) Expression of miR-135b in clinical samples of ALCL patients.